External forces direct morphogenesis and tumorigenesis of the mammary gland

by

Gautham Venugopalan

A dissertation submitted in partial satisfaction of the

requirements for the degree of

Joint Doctor of Philosophy

with University of California, San Francisco

in

Bioengineering

in the

Graduate Division

of the

University of California, Berkeley

Committee in Charge:

Professor Daniel Fletcher, Chair
Professor Tejal Desai
Professor Diana Bautista

Fall 2012

Abstract

External forces direct morphogenesis and tumorigenesis of the mammary gland

by

Gautham Venugopalan

Joint Doctor of Philosophy with University of California, San Francisco in Bioengineering

University of California, Berkeley

Professor Daniel Fletcher, Chair

Breast epithelia exist in a constant state of interaction with their surrounding environment. Morphogenesis is the developmental process by which breast cells grow into their surrounding matrix and form the ducts and milk-producing lobules. When morphogenesis breaks down, breast cancer occurs. Traditionally, biologists think of cancer through the framework of genetic mutations. Significant work in the past few decades demonstrated that the mechanical environment plays a critical role in determining growth and malignancy of breast cancers independent of genetic mutations. For example, increasing the stiffness of the extracellular matrix drives phenotypic malignancy through cell-generated contraction. However, the role of forces felt by the tissue due to external causes remains unclear. This dissertation describes experiments that reveal a critical role for external forces in branching morphogenesis and tumorigenesis. The experiments make use of a simple method to apply external compression to mammary epithelial cells embedded in biologically relevant gels.

In branching, compression mechanically aligned collagen fibers and directed multicellular branch growth along these fibers. Fiber alignment sensing required fascin activity, but did not require RhoA-mediated contraction. Contraction served a separate purpose of generating fiber alignment in collagen networks. These findings suggest that migrating cells sense fiber alignment through fascin-mediated filopodia formation rather than through RhoA-mediated contraction.

In tumorigenesis, compression encouraged malignant cells to form normal-looking acini, a process called 'phenotypic reversion.' A transient compressive force at the one-cell state was sufficient to induce reversion without genetic manipulations or pharmacological treatments. Time-lapse microscopy of the malignant cells revealed that compression restored coherent rotation of malignant cell doublets, a behavior associated with the formation of a phenotypically normal structure. Blocking E-Cadherin eliminated compression sensitivity, indicating that cell-cell communication was required for force-induced reversion.

As external forces altered the structure of a growing multicellular colony, changes in multicellular structure could affect epithelial mechanics. The mechanical properties of multicellular epithelial structures were measured using an atomic force microscope. Hollow lumen structures were softer than filled lumen structure. The increased stiffness associated with lumen filling could contribute to malignancy during cancer progression.

Taken together, this work demonstrates the importance of external forces during morphogenesis and tumorigenesis of the mammary gland. External compression can direct multicellular migration and encourage malignant cells to re-enter the 'normal' morphogenetic program. Cell-cell communication plays an important role in multicellular mechanosensing, contributing to both morphogenesis and mechanosensing in mammary epithelial structures. Further studies of multicellular mechanosensing incorporating the data and techniques presented here could identify new molecular targets for breast cancer treatment and prevention.

Table of contents

List of abbreviations

AFM	Atomic Force Microscope
Col I	Type I Collagen
DAPI	4',6-diamidino-2-phenylindole
DMEM	Dulbecco's Modification of Eagle's Medium
ECM	Extracellular Matrix
eGFP	Enhanced Green Fluorescent Protein
EMT	Epithelial-Mesenchymal Transition
EpH4	Non-malignant mouse mammary epithelial cell line
FBS	Fetal Bovine Serum
GTPase	Guanosine Triphosphate(ase)
H2B	Histone 2B
HCl	Hydrochloric acid
IL-1	Interleukin-1
IL-25	Interleukin-25
ITS-PS	Insulin, Transferrin, Sodium Selenite-Penicillin/Streptomycin
KOH	Potassium Hydroxide
MAPK	Mitogen Activated Protein Kinase
MCF10A	Non-malignant human breast epithelial cell line
MCF10AT	c-Ha-ras transformed premalignant human breast epithelial cell line
MMP	Matrix Metalloproteinase
MMP3	Matrix Metalloproteinase-3
NA	Numerical Aperture
ODE	Ordinary Differential Equation
PDMS	Poly-dimethylsiloxane
ROCK	Rho-associated Kinase
S1	HMT3522 S1 non-malignant breast epithelial cell line
SEM	Standard error of the mean
SLS	Standard linear solid
T4-2	HMT3522 T4-2 malignant human breast epithelial cell line
TGF-β	Transforming Growth Factor-β

Acknowledgements

I could never have completed graduate school without the incredible network of people supporting me over the last several years. First, thanks to Dan for taking a chance on someone who didn't really know what a pipette was for on the first day of lab. Dan was very patient as I repeatedly (and stubbornly) tried and failed at experiments, and his feedback and encouragement made a world of difference. Dan also has a great knack for bringing in enthusiastic, driven people who become the best at what they do. People in the lab were always very helpful: whether it was teaching me how to think through my problems (especially Ovi, Ross, Erik, and Lina), how to use pipettes (thanks Viv), building instrumentation (Tai-De, Clay, Ailey and Neil), making sure I have money and supplies (Stephanie and Ann) or being my foosball doormats (all of the lab). Though I didn't have a chance to work closely with everyone in the lab, I've probably asked each one of them at least 50 questions by this point.

Special thanks to Kevin for being the only one who had to put up with me for about the entire time I was here (even Dan escaped for a year). Discussing my problems with him has always been great. I'd love to continue doing so, but I think he's priced himself out of my budget…

My graduate school experience was very collaborative. The expertise of all my co-authors and colleagues taught me to approach problems in many different ways. I am especially grateful to Mina Bissell for continually supporting collaborations between our labs. It has always been great to visit the Bissell lab and get advice from everyone there who is always willing to help. I am especially grateful to Doug and Kandice for driving things forward whenever they could, and always overflowing with great ideas and unrivaled passion for research.

Thanks to my other committee members, Diana and Tejal. The feedback you provided during our discussions has always been insightful and practically applicable. Also thanks to Amy Herr and Neil Switz for designing some really great courses for me to teach, and Rebecca and the crew in the BioE office for always helping me when I walk into the office looking like a lost child.

Outside of lab, I have a wonderful network of family and friends who were always around through ups and downs. My parents and sister were always ready to listen to my rambles about whatever wasn't working and were consistently supportive through it all. I'm really excited about the cool things we've done with Future Scientist thanks to Richard and Frances and the crew; hopefully it goes somewhere from here. Anthony and the other (pent-)housemates, Richard, and all the other friends I've made during grad school were really the best part of the whole thing. Thanks for sharing the good and the bad. I'm truly impressed by the things you all have overcome to be where you are now. On that note, today is a good day to remind someone you love them before it's too late. Thanks for reading – even if you only get through the abstract.

Chapter 1: Introduction

Breast cancer is the second-most common type of malignant cancer found in women [1]. Approximately 288,000 new cases of breast cancer were expected in the United States in 2011, leading to about 40,000 expected deaths [1]. One of the reasons for the high incidence of breast cancer is its dynamic nature. The mammary gland is a unique system that undergoes significant postnatal development [2, 3]. Throughout reproductive life, the breast continuously grows and shrinks as the mother becomes pregnant, lactates, and weans new children [2]. Unfortunately, when these highly regulated multicellular growth processes fail, breast cancer occurs. A more detailed understanding of the growth

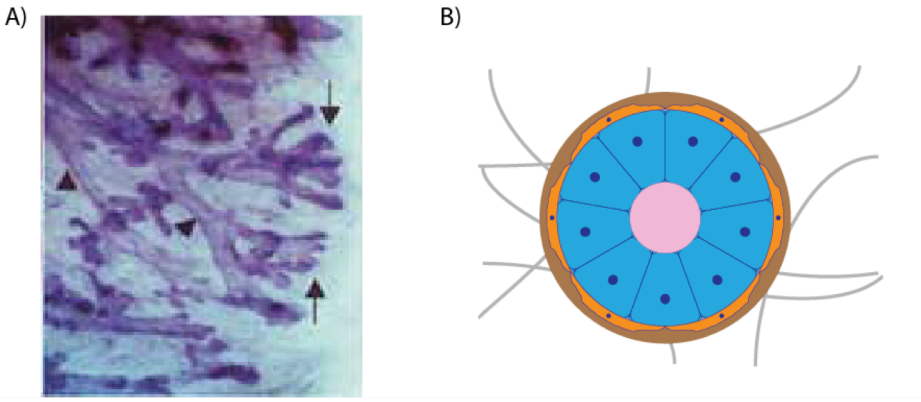

Figure 1- 1: Anatomy of the breast. A) Carmine-stained human breast epithelia. Ducts marked with arrowheads, end buds (acini) marked with arrows. From [2]. B) Cartoon of an acinus including luminal epithelial cells (blue), myoepithelial cells (orange), basement membrane (brown), lumen (pink), and stroma (grey).

processes involved in breast development could lead to new drug targets, but also inform new prevention and treatment methods.

Morphogenesis and tumorigenesis of the mammary gland

Breast development is a complex process requiring nuanced interaction between many components. For example, the surrounding extracellular matrix [4], adipocytes [5], fibroblasts [6], and macrophages [7] can impact growth of the organ. One of the most important components is the mammary epithelium itself. During puberty, the mammary epithelium grows into the fat pad of the breast to form a complex network of tubes [2] (Figure 1-1A, arrowheads). This process is known as branching morphogenesis, and forms the ductal network of the breast [2]. Following branching morphogenesis, cells near the tips of these networks grow into small, hollow lobules called acini [2] (Figure1-1A, arrows). During this acinar morphogenesis, cells form the structures used to secrete milk into the ducts. The processes involved in branching and acinar morphogenesis both have direct cancer relevance.

Branching morphogenesis

Branching morphogenesis is the developmental process by which organisms form complex, but highly-organized networks of tube-like structures used to transport fluids [8] (Figure 1-1A, arrowheads). The process involves initiation, elongation and bifurcation of new ducts [9], as well as side-branching from existing ducts[10]. In mammals, branching morphogenesis generates ductal trees in tissues such as salivary glands [11], lungs [12, 13], kidneys [14] and the mammary glands [10]. In the mammary gland, this process occurs during puberty, as a small ductal network grows into a larger one through a process of elongation and bifurcation [2]. Branching morphogenesis can be studied in culture by embedding mammary epithelial cells in a Type I collagen gel [15]. This can be done with clusters of either primary cells or a cell line [15, 16] in order to study the underlying mechanisms regulating branching.

The specific cellular mechanisms behind ductal elongation and bifurcation in mammary epithelial cell branching morphogenesis are not yet fully known [9], but a host of signaling pathways [17] and extracellular matrix (ECM) factors have been identified using a combination of *in vivo* and culture studies [10]. These studies show that factors such as integrin-ECM connections [9, 18, 19] and matrix metalloproteinases [15, 20] (MMPs) affect branching morphogenesis. General inhibition of MMPs with pharmacological inhibitors prevents branching but the effect is reversible upon washout of the drug. Addition of matrix metalloproteinase-3 (MMP3) alone is sufficient to induce branching in the absence of growth factors [15]. Mammary epithelial cells also secrete transforming growth factor- β (TGF-β) as a paracrine inhibitory signal of branching [16].

Many of the mechanisms involved in developmental branching morphogenesis are common to collective cell migration seen in cancer (reviewed by Friedl and Gilmour [21]). For example, MMPs [22], growth factor signaling [23], and contractility [24] are often seen in cancer cell collective cell migration. The epithelial-mesenchymal transition (EMT) is important for developmental processes such as branching morphogenesis [25] and gastrulation [26], but also tumor metastasis [27] and fibrosis [28]. This contributes to the theory that some cancers access developmental pathways that should be switched off in functionally differentiated cells [29].

Acinar morphogenesis

Functionally differentiated, milk-secreting end buds form on the tips of ducts during a process known as acinar morphogenesis (Figure 1-1A, arrows). During this process, cells divide and grow into a lobule, forming a large secretory cavity in the center known as a lumen [2]. Acinar morphogenesis has been studied in prostate [30], pancreas [31, 32], salivary [33], and mammary glands [34, 35, 36, 37]. End buds cyclically grow and shrink during the menstrual cycle, becoming particularly large during pregnancy and lactation [2]. During this process, acini surround themselves with a basement membrane layer rich in laminin and Collagen IV [38] (Figure 1-1B). In culture, a laminin-rich ECM can be used to study both acinar growth [34] and milk production [39].

Many important microenvironmental factors regulate acinar morphogenesis and functional differentiation. As with branching, acinus formation by healthy cells requires growth

factors [40] and integrin-ECM interaction [41]. Single breast epithelial cells do not produce milk when cultured on polystyrene [38] or Type I collagen matrices [42]. The laminin-rich ECM itself regulates functional differentiation, as breast epithelial cells grown on laminin can produce milk [38]. As a result, the associated integrins – including α_6 and β_1 – are required for growth [43] and milk production [42].

Tumorigenesis and phenotypic reversion

Malignant breast epithelial cells often overexpress these integrins, correlating with poor survival prognoses [44, 45]. When embedded in laminin-rich ECM, malignant cells form disorganized structures, but blocking β_1 integrin function causes these cells to 'phenotypically revert' and grow into structures resembling healthy acini [36]. Blocking integrin function also reduces the level of growth factor receptor expression to the level of non-malignant cells [36]. Inhibiting growth factor signaling reduces the level of β_1 integrin expression [46], suggesting a crosstalk between these integrin and growth signaling pathways. While the mechanisms of this crosstalk are still under investigation, a host of common downstream biochemical effectors have been discovered. Inhibiting cancer-related molecules like mitogen-activated protein kinase (MAPK) [46] and phosphoinositide 3-kinase (PI3K) [47] 'phenotypically reverts' malignant cells. Downstream studies showed that PI3K controls polarity and proliferation through separate mechanisms in breast epithelial cells [47].

These experiments with pharmacological inhibitors demonstrate the importance of the local microenvironment in tumor growth. Malignant breast epithelial cells treated with these inhibitors can take on a phenotypically normal appearance even though they remain genetically unchanged. Understanding cellular interaction with the microenvironment is a very promising concept for cancer treatment. If cancer cells could be 'reverted' to behave normally *in vivo*, it would provide new avenues for treatment and management of malignant tumors. For example, pharmacological inhibitors of growth factor receptors [48] and integrins [49] have been investigated as potential cancer therapies.

Microenvironmental mechanics in mammary morphogenesis and cancer

Given the importance of integrin specificity and ECM ligand presentation, it may not be surprising that physical cues from the microenvironment affect cellular behavior. Resistance training increases leads to hypertrophy of muscle [50, 51], and bone remodels in response to mechanical cues [52]. Musculoskeletal development also depends on ECM stiffness. Mesenchymal stem cells differentiate into bone, muscle, or neuron cells depending on the stiffness of the underlying matrix [53]. The cellular machinery involved in this process is conserved across many cell types [54], and ECM stiffness is a key regulator of other developmental processes including morphogenesis of the mammary gland.

Matrix stiffness regulates acinar morphogenesis

Increasing the stiffness of this ECM would increase the force exerted by a cell during contraction [55], and could couple into growth-related processes [56]. Acinar morphogenesis normally takes place in native breast tissue, a soft environment with

stiffness on the order of ~100 Pa [57]. Because breast tumors are much stiffer than healthy tissue (~2000 Pa), Paszek and colleagues grew non-malignant breast epithelial cells on soft and stiff matrices to investigate the effects of stiffness on acinar morphogenesis [57]. Non-malignant cells form phenotypically normal acini on soft matrices, but on stiff matrices form disorganized, non-polarized structures. Despite remaining genetically 'normal,' non-malignant cells on stiff substrates exhibit increased integrin clustering and contractility. Genetically malignant cells already have increased integrin clustering and contractility, but inhibiting contractility with pharmacological agents leads to 'phenotypic reversion' of the malignant cells. Downstream of integrin clustering, pharmacological inhibition of focal adhesion kinase prevents tumor formation in mice [58], and is a potential cancer therapy.

Mammary epithelial cells also require the correct stiffness to produce milk. Alcaraz and colleagues measured the stiffness of primary mammary epithelial cell clusters (organoids) to be approximately 500 Pa [42]. They discovered that single mammary epithelial cells plated on soft polyacrylamide gels also exhibit similar stiffness. However, when plated on stiffer gels (~50kPa), these cells are 3-fold stiffer than the normal phenotype. With this increase in stiffness comes a loss of β-casein expression. Cells on the soft gels express a fluorescent reporter tied to β-casein expression, but cells on stiffer gels lose this expression [42]. Like acinar morphogenesis, functional differentiation was also associated with actomyosin contractility, as cells plated on laminin-rich ECM exhibit decreased phosphorylation of non-muscle myosin II [42]. Although the authors measured the stiffness of single cells and multicellular colonies, it is not known whether the multicellular architecture formed by the cells plays any role in stiffness sensing.

Matrix stiffness and matrix organization direct cancer cell invasion

Cell-ECM mechanics also play a role in branching morphogenesis and cancer cell invasion. Cells migrate along small ridges and features [59] and proliferation is reduced on arrays of small pegs [60]. Cells plated on polyacrylamide gels with a stiffness gradient tend to migrate towards the stiffer direction, a process called durotaxis [61]. Dense collagen is stiffer [62], and aligned collagen fibers are stiffer in the aligned direction [63], so durotaxis predicts that cell migration would preferentially follow dense, aligned fibers.

Collagen alignment correlates negatively with survival in breast cancer [64], and increasing collagen density increases the likelihood of breast tumor formation and metastasis [65]. Ex vivo microscopy confirms that collagen alignment associates with tumor invasion [66], while stiffening via matrix crosslinking promotes an invasive phenotype [4]. Epithelial cancers often become invasive through a process called collective cell migration, where a group of cells follow a 'tip' or 'leader' cell through the matrix [21]. Tip cells remodel the matrix, aligning fibers at the leading edge towards the collective cell migration direction [21]. Actomyosin contraction-mediated alignment of collagen fibers promotes tumor migration in culture [67]. This evidence suggests that migrating cells realign collagen fibers using similar contractile machinery as stiffness sensing. Cells also tend to follow aligned collagen fibers. However, it remains unclear if alignment generation and alignment following utilize different molecular machinery.

External forces

In addition to stiffness and matrix organization, cells experience a host of externally applied stresses and strains in their native environment. These forces can be due to environmental factors such as neighboring cell contraction [68] or fluid flow [69]. Single cells directly respond to external forces (e.g. [70]), and interesting behaviors have been observed at the multicellular level. For example, two-dimensional epithelial sheets migrate more under external compression, but only if they consist of malignant cells [71]. In three dimensions, cancer cell aggregates embedded in agarose respond to mechanics. Increasing compression promotes apoptosis and results in a smaller critical tumor size [72, 73]. This growth/apoptosis balance has also been computationally investigated [74], and the body of work suggests that external compression could check the growth of a normally unstable tumor.

These studies performed on pre-aggregated tumor spheroids in agarose provide insight into the phenomenon of tumor growth. However, a number of key questions remain unresolved. Mammalian cells cannot interact with agarose using integrins and MMPs. Integrin clustering promotes malignancy through cell-ECM interaction [4, 57], but the role of external forces on malignancy in a biologically relevant ECM remains unknown. While single breast epithelial cells form acini in culture, pre-aggregated cells do not [75], suggesting that the manner in which cells are connected significantly alters their ability to form polarized structures. An investigation into the effects of external forces on morphogenesis and malignancy is needed to address some of these questions.

Studying morphogenesis and tumorigenesis in culture

Many of the experiments described above used three-dimensional culture models to mimic morphogenesis and tumorigenesis of breast epithelia. These experiments are generally performed with epithelial cells embedded in reconstituted ECM gels. Careful selection of appropriate cell lines and ECM proteins allows for the study of branching morphogenesis, acinar morphogenesis, and tumorigenesis in culture.

Branching morphogenesis in culture

At the onset of branching morphogenesis, a small cluster of cells begins to invade together into the surrounding, matrix composed primarily of adipose tissue and Type I collagen [2]. Clusters of primary cells extracted from mice are known as ‘organoids’ and undergo branching when embedded in reconstituted Type I collagen gels (collagen usually derived from rat tail) [15]. Branching can also be studied in culture using ‘aggregates’ of the non-malignant EpH4 or SCp2 mouse mammary epithelial cell lines [10, 15]. Both aggregates and organoids require similar MMP function and make similar-looking branches in culture [15]. These clusters are especially useful for studying the multicellular migratory component of branching morphogenesis, including studies of branch direction [16].

Acinar morphogenesis and tumorigenesis in culture

In contrast to branching, acinar morphogenesis and milk production occur primarily in a laminin and Type IV collagen basement membrane [38]. As a result, acinar morphogenesis is studied in culture by embedding mammary epithelial cells into a laminin-rich ECM, an ECM usually extracted from Engelbreth-Holm-Swarm sarcomas in mice (e.g. Matrigel™)

[76]. Single human breast epithelial cells embedded in (or grown on top of) laminin-rich ECM form acini resembling the milk-producing end buds found *in vivo* [34, 36]. Starting with single cells in this assay is particularly important to study structure formation and growth, two crucial behaviors during acinar morphogenesis. The cells most commonly used are either primary cells [75] or non-malignant cell lines such as HMT3522-S1 [36], or MCF10A [34]. HMT3522-S1 cells form growth-arrested, polarized acini [35], whereas MCF10A acini do not growth arrest, forming larger structures [34].

Malignant single cells can also be embedded in laminin-rich ECM to study tumorigenesis. Malignant cells form disorganized tumor-like colonies in culture [36, 77]. Extremely metastatic lines like MCF-7 [78] and MDA-MB-231 [79] are useful for studies of invasiveness, but are difficult to compare directly to non-malignant morphogenetic behaviors. To make these comparisons, progression series such as MCF10A/AT/CA1, and HMT3522-S1/T4-2 are useful. The MCF10AT line is a Ras-oncogene transfected 'pre-malignant' line [80, 81] that forms filled acinar structures in culture [82]. Because MCF10AT cells are the result of a defined genetic transfection, the differences between MCF10A and MCF10AT lines are fairly well defined, though not very drastic. The MCF10AT cells were repeatedly xenografted into mice to generate malignant MCF10CA1 cells [83], which can be used to study malignant progression. Similarly, HMT3522-T4-2 cells are a growth-factor-independent malignant cell line grown from HMT3522-S1 cells [77]. The HMT3522-S1/T4-2 progression is particularly useful for understanding the factors involved in promoting/inhibiting malignancy independent of genetic mutations. Malignant T4-2 cells can be 'phenotypically reverted' to growth-arrested, organized structures resembling the non-malignant S1 structures (as reviewed above).

Techniques for manipulating the mechanical microenvironment of cells

Several existing techniques can be used to manipulate the mechanical microenvironment of cells independent of genetic mutations. These techniques fall into four broad categories, pharmacological inhibition, cell patterning, matrix modifications, and applied forces. This section highlights some of these techniques, primarily in the context of breast morphogenesis and tumor growth. A complete review is beyond the scope of this work, but the information can be found in the literature [84, 85, 86, 87, 88].

Pharmacological disruption of mechanosensing

One of the most common ways to modify the mechanical microenvironment is to disrupt mechanosensing machinery using pharmacological inhibitors. Pharmacological inhibitors are usually added directly to the cell culture medium. Three inhibitors used to study mammary epithelia are contractility inhibitors [42, 57, 75], function-blocking antibodies [36, 75, 89], and focal adhesion kinase inhibitors [58]. In non-malignant cells, contractility inhibition prevents the formation of spherical acinar structures [75], while in malignant cells it promotes phenotypic reversion [57]. Function blocking E-cadherin prevents acinus formation [89], while blocking β_1-integrin phenotypically reverts malignant cells [36]. Inhibiting focal adhesion kinase inhibits tumor growth *in vivo* [58].

Patterning to regulate cell shape

Soft lithography fabrication technology was adapted to create patterns of adhesive regions of controlled size and shape. The process known as micropatterning can be used to generate patterns with just about any ECM protein, at sizes ranging from sub-micron to hundreds of square microns [90, 91]. Initial micropatterning techniques used an elastomeric stamp to pattern hydrophobic alkanethiols into a self-assembling monolayer on a gold or silver surface [92]. The remaining space was filled with a self-assembling monolayer of hydrophilic alkanethiols. The protein of interest was then stuck to the surface by hydrophobic interactions, and remaining exposed areas were blocked with nonadhesive substances. Alternate versions of this technique eliminated the need for self-assembling monolayers [93], allowing researchers to use glass coverslips and a larger array of imaging modalities. Early studies on micropatterned substrates focused on the relationship between cell shape and apoptosis [90].

Micropatterning has been used to study branching morphogenesis in two- and three-dimensions. MMP3 treatment of individual mammary epithelial cells induces EMT [94]. Limiting cell spreading in 2D by using smaller patterned areas inhibits expression of EMT markers when cells are treated with MMP3, but not with TGF-β – a small molecule that can trigger EMT via alternate pathways [94, 95]. A three-dimensional analogue to micropatterning uses elastomeric stamps to make microwells in collagen gels and embed cells clusters in the wells [16]. The shape of the microwell determines the shape of the cell cluster. Branches form in positions around the cluster in a fashion predicted by diffusion-mediated paracrine inhibition via TGF-β.

Matrix modifications to regulate stiffness and microstructure

When culturing cells in collagen matrices, stiffness of the ECM can be simply increased by increasing the collagen concentration [57, 62]. However, this increases matrix ligand density [96] and potentially changes matrix microstructure [97]. A number of techniques have been developed to modulate ECM stiffness independent of ligand density, including collagen-agarose mixtures [98], alginate gels [99], and coated atomic force microscopy (AFM) cantilevers [100]. By far the most common way to change stiffness of the ECM is to plate cells on polyacrylamide gels. The stiffness of the gel can be modified by adjusting the ratio of acrylamide and the bis-acrylamide crosslinker [101]. An ECM protein can be covalently attached to the top of the gel at a desired ligand density [102]. This technique has been used to study many behaviors including differentiation [53] and motility [61].

In breast morphogenesis, polyacrylamide gels have been used to study functional differentiation [42], and to show that yes-associated protein localizes to the nucleus on stiff substrates [103]. Studying stiffness and acinar morphogenesis proves more difficult, as cells must be grown in laminin-rich ECM to undergo morphogenesis. Cells embedded cells in a thin layer of laminin-rich ECM on top of a polyacrylamide gel will still feel the stiffness of the gel [57]. As described in detail above, this method was used to demonstrate that increased stiffness drive phenotypic malignancy. Stiffness-mediated mechanotransduction in breast continues to be extensively studied, but applied forces have received less attention.

Applied forces

Applying forces to tissues in vivo is difficult, but animal models exist to study musculoskeletal mechanics [104, 105] and chronic nerve compression [106]. In order apply more defined loads (and save some animals), there are several ways to apply forces directly to cells and tissues in vitro (several reviewed by Brown [88]). For example, AFM cantilevers [70, 107], optical traps [108], and magnetic beads [109] can been used to directly apply forces to single cells [110] and subcellular components [111, 112]. Cells can also be plated on flexible membranes and cyclically strained for long times [113]. In breast epithelial cells, cyclic stretch induces phosphorylation of focal adhesion kinase [114]. Micropipette aspiration can be used to probe single cells [115] or multicellular aggregates [116]. Experiments where forces are directly applied to cells are particularly suited for identifying fundamental behaviors of cytoskeletal and mechanosensing machinery.

Multicellular and tissue mechanics are of particular interest in morphogenesis and tumor growth. A compression platen can be used to directly apply forces to tissue explants or cell-embedded matrices [117]. Constant compression by platen has been used to study mechanobiology of cell sheets [71] and aggregates [73]. Bioreactors with hydrostatic pressure can also be used to apply long-term forces to tissue explants or cell monolayers [118]. Platen systems are especially good for uniaxial tests and working in strain space, while hydrostatic systems can be useful for bulk compression and working in stress space.

Some of these systems are capable of long-term culture (e.g. [73]), but a low-cost, high-throughput, microscopy-friendly method to apply compression to cells embedded in biologically relevant ECM gels would allow for in depth study of the complex mechanical processes involved in morphogenesis and tumorigenesis of the mammary gland.

Scope of the present study

Many open questions remain in the study of branching morphogenesis, acinar morphogenesis, and tumorigenesis. This dissertation investigates three of these questions:

1. How do mouse mammary cell aggregates sense mechanically induced collagen fiber alignment during branching morphogenesis?
2. How does transient compression alter the malignant phenotype of human breast epithelial cancer cells during tumorigenesis?
3. How could multicellular architecture play a role in mechanical property changes observed during lumen filling in cancer progression?

To investigate the first two questions, I develop a silicone culture system to apply compressive strains to cells embedded in ECM gels. The system allows for culture in a standard cell culture incubator or on a time-lapse microscope. It is low cost (~$6 per test at current silicone prices) and many samples can be run in parallel without specialized hardware. Working with my collaborators, I use this silicone compression system to study the effects of external compression on branching morphogenesis (Chapter 2) and tumorigenesis (Chapter 3) of the mammary gland. In Chapter 4, we further investigate the effects of loss of structure on the mechanical properties of a multicellular tissue subunit. This work concludes with a discussion of future lines of experimentation that would further our understanding of the mechanics of breast development and tumorigenesis.

Chapter 2: Patterned collagen I directs branching morphogenesis of the mammary gland

With:
Mina J. Bissell[2]
Douglas G. Brownfield[1,2]
Daniel A. Fletcher[1,3]
Alvin Lo[2]
Hidetoshi Mori[2]
Kandice Tanner[2]

[1] Department of Bioengineering, University of California, Berkeley, CA

[2] Life Sciences Division, Lawrence Berkeley National Laboratory, Berkeley, CA

[3] Physical Biosciences Division, Lawrence Berkeley National Laboratory, Berkeley, CA

Abstract
Organs are comprised of tubular networks critical for the transport of cells, fluids, and gases [119]. Although previous work has demonstrated the mesenchyme's striking ability to instruct epithelial form and function [120, 121, 122], little is known about the role of extracellular matrix (ECM) molecules in pattern specification. Here we show that stromal collagen (Col) fiber orientation plays a key role in directing epithelial organization. In the mammary fat pad, Col fibers are axially oriented prior to branching morphogenesis. Upon puberty, the branching epithelium orients along these fibers thereby adopting a similar axial bias. To test whether there was a causal relationship between Col fiber organization and epithelial orientation we embedded mammary organoids within axially oriented Col I fiber matrices in culture and observed robust epithelial co-orientation. In contrast, we saw no directional preference in randomly oriented Col I fiber matrices. Constitutive activation of Rac1, a regulator of cell motility, disrupted epithelial sensitivity to Col I fiber orientation. Interestingly, inhibition of the RhoA/Rho-associated kinase (ROCK) pathway did not affect epithelial sensitivity to Col I fiber orientation, but time-lapse studies revealed that the epithelium can axially orient non-aligned Col I fibers at branch sites via RhoA/ROCK-mediated contractions. Our data provides an explanation of how the stroma encodes architectural cues for branch orientation that the branching epithelium interprets and reinforces through molecularly distinct processes.

Results

Mammary epithelial branches co-orient to aligned collagen fibers in the stroma

Mammary epithelial orientation was measured at early (Figure 2-1A, postnatal week 3) and late stages (Figure 2-1A, postnatal week 8) of branching morphogenesis. We observed no stereotyped orientation pattern in early stage mammary glands, with epithelia randomly distributed along either the short- (Figure 2-1A, ±90˚) or long- axis (Figure 2-1A, 0˚; 1B). In contrast, the late stage epithelial pattern was stereotyped and displayed a significant orientation along the long axis of the mammary gland (Figure 2-1A 0˚; 1B). Since epithelial orientation was axially biased after substantial outgrowth into the previously unexplored stroma, we hypothesized that a stromal patterning cue for orientation may already be present in the mammary fat pad. We chose Col as a candidate patterning cue since previous work with macrophages shows the presence of Col I fibers proximal to the mammary epithelium [123]. Additionally, malignant cell migration occurs on or around Col I fibers [64, 66], though little is known about the role of endogenous oriented Col I bundles in interacting with the developing mammary epithelium.

We analyzed Col organization at sites distal to the epithelium within early stage mammary glands (Figure 2-1C, dashed box). Visualizing Col at different depths, we observed layers of varying intensity as well as organization (Figure 2-1C, High-Low). High intensity regions were located proximal to the fascia, whereas medium intensity regions were located at different depths (Figure 2-1C, XZ). Both high and medium intensity regions contained fibers significantly oriented toward the long axis (Figure 2-1D). In contrast, low Col staining intensity was located in the stroma at adipocyte-rich regions containing no fibers and displayed no discernible orientation bias (Figure 2-1C, Low; 1D).

We examined Col organization proximal to early stage mammary epithelia and observed significantly higher fiber intensity at both ducts and end buds (Figure 2-1E). The latter exhibited fibers persisting approximately 300μm ahead of the epithelium, demonstrating that in vivo Col fibers are formed prior to their association with the epithelium (Figure 2-1E). The Col fibers proximal to end buds displayed a co-orientation to branch direction (Figure 2-1F). These data suggested that Col fibers might encode patterning cues within the extracellular space of the mammary gland prior to branching of the epithelium.

Collagen I fiber orientation is sufficient to direct branching

To test whether there was a causal relationship between Col I fibers and epithelial orientation, we developed a novel method (Figure 2-2A) for generating an axial orientation bias in Col I matrices before induction of branching in 3D culture. Malleable wells were fabricated from polydimethylsiloxane (PDMS) and stretched along one axis. A liquid mixture of Col I and mammary epithelial cells was prepared as previously described [15] and added into the pre-stretched PDMS wells. Upon Col I matrix polymerization, we gently released the PDMS wells to generate a uniaxial compression (~20% strain), inducing a significant axial orientation pattern compared to control (randomly oriented) matrices that was confirmed by confocal reflection (Figure 2-2B-D). Stress relaxed in compressed Col matrices with a characteristic relaxation time constant on the order of 5s, orders of

magnitude faster than the time to form branches (Figure 2-3A). Col matrices stiffened somewhat in response to 20% shear strain (Figure 2-3B), a strain-stiffening behavior consistent with strain-induced fiber alignment [63].

To determine whether Col I fiber orientation was sufficient to direct branch orientation, organoids were embedded in either patterned or control Col I matrices (Figure 2-2E-F). Whereas organoids branching in control Col I matrices showed no orientation bias, we observed axially oriented branching in patterned Col I matrices (Figure 2-2G) providing strong evidence that Col I fibers impart directional cues to branching mammary epithelial cells.

Rac1 Activity modulates epithelial co-orientation to Col I fibers

Using our patterned Col I branching assay, we sought to identify components critical to co-orientation. Initial time-lapse experiments showed frequent and repeated cellular protrusions at branch sites proximal to patterned Col I (not shown), inferring an involvement of the cell's motility machinery with orientation sensing. We therefore chose to modulate this behavior by activating Rac1, a GTPase shown to regulate lamellipodial protrusions through local remodeling of both the actin cytoskeleton and focal adhesions [124, 125]. Expression of a constitutively-active form of Rac1 (Rac1-CA) disrupted branch orientation of mammary epithelial aggregates significantly compared to vector alone (Figure 2-2I-K). Branch morphology also was altered in Rac1-CA aggregates, which increased in the number of short multicellular branches that terminated in long cellular protrusions (Figure 2-2J, arrow). Conversely, we tested whether expression of fascin-1, a factor downstream of Rac1 that stabilizes some actin-based protrusions by tightly bundling actin [126], could increase sensitivity to Col I fiber orientation. When aggregates expressing fascin-1 were embedded in axially patterned Col I matrices (Figure 2-2L-N), we observed a modest, though not significant, enhancement in sensing Col I orientation. From these data we infer that epithelial sensitivity to oriented Col I fibers is Rac1 dependent.

ROCK-mediated contractions are required for generating, not sensing Col I fiber orientation

The dynamic interactions between Col I fibers and branch orientation were captured by time-lapse experiments on mammary epithelial organoids embedded in randomly oriented Col I matrices. We established a time window for comparing Col I orientation at the early stage prior to branching, when the Col I matrix is randomly oriented (Figure 2-4A, 28 hours), to the late stage in which substantial branching had occurred already (Figure 2-4B, 39 hours). Visualizing Col I fibers by confocal reflection microscopy, we observed local contractions at branch sites at the early stage (Figure 2-4A and 3B, inset) leading to an increase in Col I fiber co-orientation by the late stage (Figure 2-4C). These results indicate that in the absence of patterned Col I fibers, mammary epithelial cells can generate their own oriented Col I paths via contractions. Suspecting the involvement of RhoA/ROCK signaling in mediating actomyosin contractions [127], we inhibited ROCK with Y-27632, a small molecule inhibitor, and confirmed interrupted contractions in our assay (20μM, Figure 2-5A-C). Treatment of mammary epithelial aggregates with the inhibitor significantly disrupted Col I orientation at epithelial branches compared to vehicle alone (Figure 2-4D-F). These data demonstrate that branching mammary epithelial cells are capable of enhancing Col I co-orientation via ROCK-mediated contractions.

In studying RhoA/ROCK-mediated contractions with respect to generating Col I patterns, the above observations were made in randomly oriented Col I matrices. To determine whether such contractions were also involved in sensing Col I fiber orientation, we embedded mammary cells in patterned Col I matrices. In this context, no significant difference in branch orientation was observed between Y-27632 (20μM) and vehicle treatment (Figure 2-4G-I). In addition, we inhibited RhoA activity through expression of a dominant negative form of RhoA (RhoA-DN). We found no significant change in branch orientation between aggregates expressing RhoA-DN and vector control (Figure 2-4J-L), consistent with results from Y-27632 experiments. From these data, as well as from studies where we inhibited molecules further downstream in the RhoA/ROCK pathway (Figure 2-5D-G), we concluded that during branching morphogenesis the role of actomyosin contractions is restricted to enhancing Col I fiber orientation proximal to branch sites.

Discussion

The question of whether patterning cues are present in the stroma prior to epithelial branching morphogenesis is unresolved despite cumulative evidence demonstrating the significance of interactions between the epithelia and stroma during development [10, 120, 121, 122, 128, 129, 130, 131, 132, 133, 134]. Here we show that Col fibers are oriented in the mammary fat pad long before the initiation of branching morphogenesis. This observation suggests the intriguing possibility that epithelial architecture may be pre-patterned in the stromal microenvironment in vivo. A previous study has highlighted the possible involvement of macrophages in fibrillogenesis proximal to the branching epithelium [123]. Although they reported that macrophage deficiency leads to aberrant terminal end bud morphology [123], they did not explore whether macrophage-mediated fibrillogenesis directed the epithelial orientation. We hypothesized that the pre-patterned Col fibers proximal to, and that extend ahead of, the branching epithelium were likely important contributors to directional cues for the epithelium.

We demonstrated that stromal fiber orientation directs epithelial branching using a 3D culture model in which a Col I matrix is axially patterned by the application of mechanical strain. While previous studies characterizing Col I matrix structure in culture [63, 117, 135] and in vivo [136] show linear relationships between mechanical perturbations and fiber alignment, our method shows that approximately 20% strain was sufficient to align fibers and observe significant differences in branch orientation. Accordingly, our assay was sufficient to discern 'path-finding' from 'path-generating' mechanisms during branching morphogenesis.

We identified Rac1 as a critical component involved in sensing Col I orientation during branching morphogenesis. Rac1 has been implicated in directional persistence during single-and collective-cell migration [137, 138, 139]. The interaction between fascin-1 and Protein kinase C within protrusions during cell migration is Rac1-dependent [140, 141, 142]. Intriguingly, our analysis of previously published gene expression profiling of the branching mammary epithelium [25] revealed a significant increase of genes involved in the Rac1/fascin-1 axis at the end buds versus the ducts (fold-increase: *Fscn1* 2.1, *Iqgap1*

1.7, *Racgap1* 2.5, *Itga5* 1.7, and *Sdc1* 2.7; data not shown). These data additionally support the involvement of Rac1/fascin-1 signaling in branching morphogenesis at the migratory front where Col I sensing presumably occurs.

The role of RhoA/ROCK signaling in branching morphogenesis had remained unclear from previous studies. Studies using culture models demonstrated the involvement of ROCK in sensing Col I stiffness as well as tubular pattern self-assembly [127, 143], whereas studies in vivo where RhoA is inactivated within the mammary epithelium failed to inhibit branching [144]. By separating the processes of fiber patterning from sensing orientation, we now have reconciled these seemingly dissonant observations. Our results demonstrated that RhoA/ROCK-mediated contractions are not necessary to sense Col I fiber orientation. However, we observed that these contractions enhance local Col I orientation. Thus, the capacity of mammary epithelium to generate actomyosin contractions could be important for reinforcing directional decisions during branching morphogenesis. Future work in vivo is necessary to confirm this possibility as well as to determine where along the epithelium contractions occur. It has been shown that end buds express P-190B, a factor that inhibits RhoA activity; therefore, contractions most likely occur proximal to, or within, ductal epithelium where RhoA activity is required for repolarization [9].

Our present study provides strong evidence that epithelial orientation is pre-patterned by stromal Col I fibers prior to the initiation of branching morphogenesis. We show that the machinery employed by the epithelium to sense Col I fiber orientation is molecularly distinct from those that generate Col I alignment. Our findings emphasize that stromal patterning as well as orientation sensing of the extracellular milieu are critical processes in determining the architecture of epithelial tissues. Future work will aim to characterize how such Col fiber patterns are generated and which cell types are involved in stromal patterning.

Methods

Animal experiments

Animal housing, care, and experiments were performed under federal guidelines and approved by Institutional Animal Welfare and Research Committee at Lawrence Berkeley National Laboratory.

Whole mount preparation and staining

The inguinal mammary glands (#4 and #9) were extracted from either 3 or 8 week old female Balb/c mice and allowed to attach on Superfrost Plus glass slides (Fisher Scientific). Samples were fixed with Carnoy's solution (75% ethanol and 25% glacial acetic acid) overnight, stained with carmine alum, and destained (2% HCl in 70% ethanol) for no less than 16 hours. Stained samples were dehydrated by in solutions of increasing ethanol concentrations (70%, 80%, 90%, 95%, and 100%) for 30 minutes each before defatting by addition of Xylene for 48 hours. Prepared glands were mounted in Permount (Fisher Scientific, Pittsburgh, PA) under a coverslip and left to dry for 48 hours before further processing.

To visualize Col organization, a fluorescent probe was generated as previously described [145, 146]. Briefly, the vector pQE30CNA35, coding for the collagen binding part of the A domain of Staphylococcus aureus collagen adhesin (CNA35) fused to an N-terminal His tag (a kind gift from Magnus Höök , Texas A&M University), was transformed into the BL21 *E.coli* strain (Invitrogen). Protein expression was induced during liquid culture by addition of 1 mM isopropyl-β-d-thiogalactopyranoside (IPTG) for at least 4 hours before purifying the his-tagged recombinant protein via manufacturer's guidelines (Ni-NTA columns, Qiagen). Purified CNA35 was labeled with succinimidyl Alexa Fluor 564 following the manufacturer's instructions (Invitrogen). Extracted mammary glands were incubated after Carnoy's fixation with labeled CNA35 (1:100) overnight in PBS at 4˚ C before washing, dehydration, and defatting steps.

Branching assay and Col I matrix orientation

Primary organoids for time lapse experiments as well as initial work with oriented Col I matrices were isolated as described previously [147]. Briefly, 4 to 8 mammary glands were removed from 10-week female virgin Balb/c mice and minced with two parallel razor blades. Minced tissue was incubated in digestion buffer (2 g/l trypsin, 2 g/l collagenase type-iv, 5% fetal bovine serum (FBS), 5 μg/ml insulin in cultured in a 1:1 mixture of Dulbecco's Modified Eagle and Ham's F-12 medium (DMEM/F12)), centrifuged and washed at least three times to remove both residual fat as well as non-epithelial cell types, leaving a final pellet enriched in epithelial clusters.

For experiments in which transgenic expression or pharmacological inhibition was necessary, aggregates of the EpH4 cell line were prepared [148]. EpH4 cells were cultured in DMEM/F12 supplemented with 10% FBS and 1% Gentamicin at 37˚C in a humidified 5% CO_2 incubator. For aggregation, EpH4 cells were trypsinized and plated on nonadhesive wells (polyHEMA, Sigma) at a density of 800 cells per mm^2. The aggregating cells were cultured in DMEM/F12 supplemented with insulin, transferrin, selenium, and penicillin-streptomycin (ITS-PS) for 48 hours before being embedded in Col I matrices.

Col I matrices were prepared from acid-soluble rat tail collagen I following manufacturer instructions (BD Biosciences) to a final concentration of 3mg/ml before the addition of either organoids or aggregates at the concentration of 1 cluster/μl. The mixture was added to 48-well Falcon plates or PDMS wells of equal dimension (300μl per well) and incubated for 45 minutes at 37˚C. After sufficient Col I polymerization, DMEM/F12-ITS-PS (600μl per well) supplemented with 9nM bFGF (total volume, R&D Systems) was added to induce branching. Media was replaced every 2 days. After three days branching clusters were either imaged directly or fixed and stained with DAPI and Phalloidin as previously described [37]. For time-lapse studies, smaller Col I matrices (100μl) were polymerized in 8-well chambered #1 coverglass (Lab-Tek).

To orient Col I matrices, PDMS wells were fabricated from an acrylic master with dimensions matching a 48 well plate at a ratio of 10:1 of base:curing agent (Sylgaard 184, Dow Corning). The wells were then removed from the master, UV oxidized for 7 minutes (UVO-Cleaner42, Jetlight Co.), rinsed with distilled H_20 under vacuum overnight, and dried. To generate an axial orientation with 3D collagen matrices, PDMS wells were stretched

prior to addition of collagen using custom-made acrylic frames and steel pins (McMaster-Carr). After polymerization the pins were removed, generating 20% axial compressive strain.

Plasmids and Inhibitors

Lentiviral plasmids were constructed from pLenti Puro DEST such that the elongation factor 1 alpha (EFS) promoter drove expression of either N-terminal CyPet labeled $Rac1^{Q61L}$ (Rac1-CA) or N-terminal labeled YPet $RhoA^{T17N}$ (RhoA-DN). Lentiviral production, infection, and subsequent antibiotic selection were conducted to manufacturer's protocol (Virapower Lentiviral Gateway, Invitrogen). Fascin-1 was expressed using the lentiviral plasmid pCDH (System Biosciences). For specific inhibition of ROCK, Y-27632 (Tocris) was added to Col I mixture prior to polymerization as well as afterwards in the media to the final concentration of 20μM.

Microscopy and orientation analysis

Carmine stained whole mounts were imaged using a Zeiss Stereoscope. For quantifying branch orientation, brightfield images were taken on a Zeiss Axiovert with a 0.45 NA 10X air objective. Imaging of Col probe fluorescence as well as confocal reflection was performed on a Zeiss LSM 710 using a 1.1 NA 40X water-immersion objective. For time-lapse experiments, samples were maintained at 37 °C and 5% CO2.

To quantify in vivo branch orientation, epithelial traces were generated using ImageJ (NIH) and orientation was measured in 50μm intervals using a custom Matlab script (Mathworks), with a minimum of 300 measurements per gland and 10 glands sampled per time point. Branch orientation in culture was measured from cluster's geometric center to branch end via ImageJ, with a branch determined as twice the length of the cluster's base width. At least 50 clusters measured per condition, totaling about 150-250 branch measurements per condition. Collagen orientation was measured using OrientationJ, an ImageJ plugin [149]. Statistical analysis was performed with Sigmaplot and plots generated using Matlab (Mathworks).

Acknowledgements

We are grateful to Saori Furata for valuable discussion and critical reading of the manuscript. We also thank all other members of the Bissell as well as Fletcher laboratory for comments and discussions. We wish to thank Sanjay Kumar and Joanna MacKay for sharing image correlation MATLAB code.

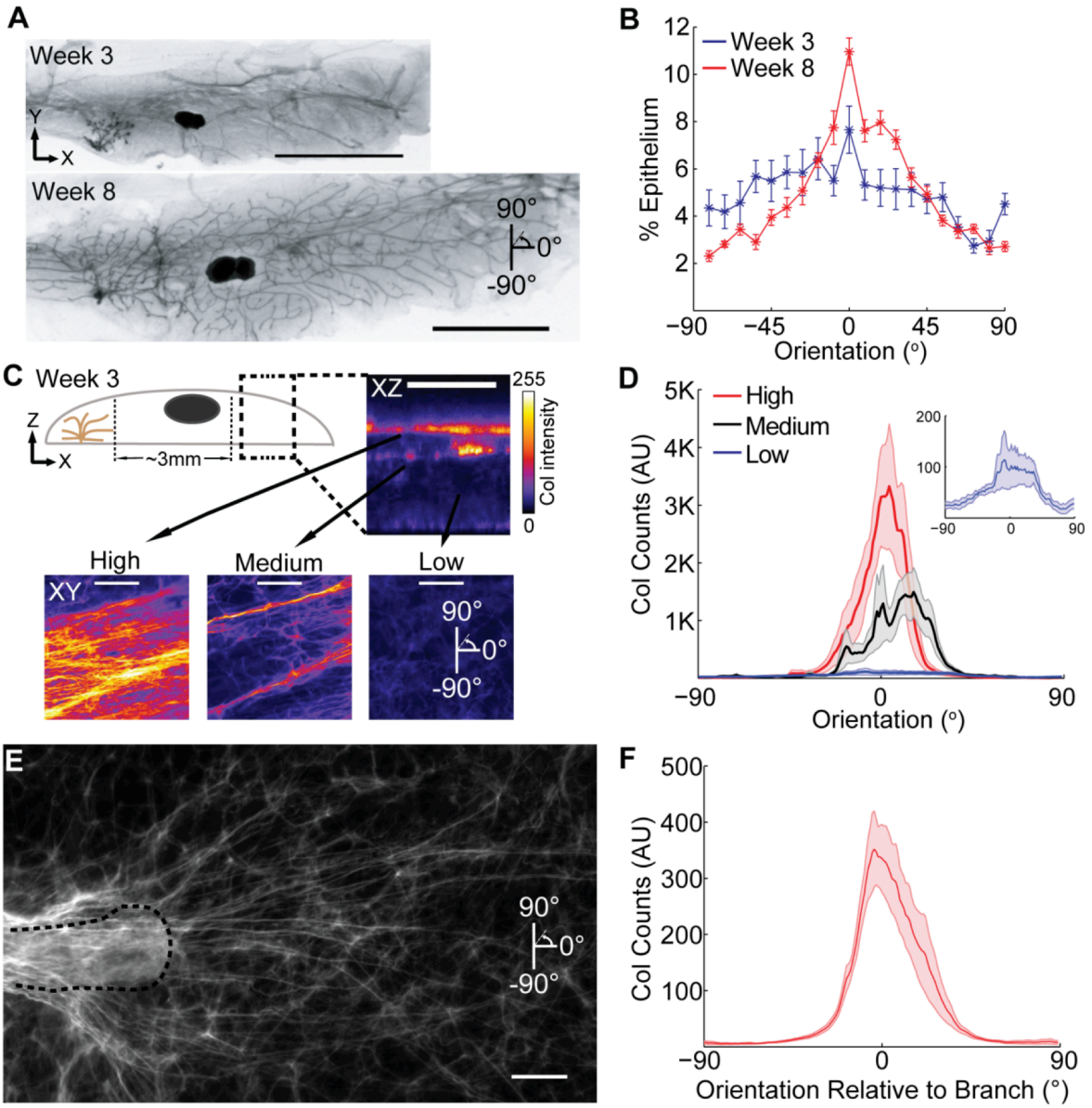

Figure 2-1: Axial Col tracks orient the branching mammary epithelium. Representative mouse mammary gland whole mounts at postnatal week 3 and 8 (A). Branch orientation analysis of traced epithelia showed a transition from an unbiased structure at 3 weeks to one significantly orientated along the 0˚ axis by 8 weeks (B); values are mean ± SEM, n=10-11 (whole mounts). Fluorescently labeled Col tracks in week 3 mammary glands were visualized at sites distal to the epithelium (C, dashed box). Col signal at various depths distally show layers of high, medium, and low intensity, with medium to high areas containing the majority of Col fibers (C). Fiber orientation analysis (D) of these regions revealed a significant orientation bias towards the 0˚ axis in high and medium regions while low intensity region had no significant bias; values are mean ± SEM, n=5. Col fibers proximal to the epithelium at week 3 extend past and co-orient to branches (E). Col fiber orientation analysis (F) at branch sites of week 3 mammary glands found Col fibers co-oriented with branch direction; values are mean ± SEM, n=5. Scale bar in (A,G) represents 5mm; scale bars in (B-E, I) represent 50μm

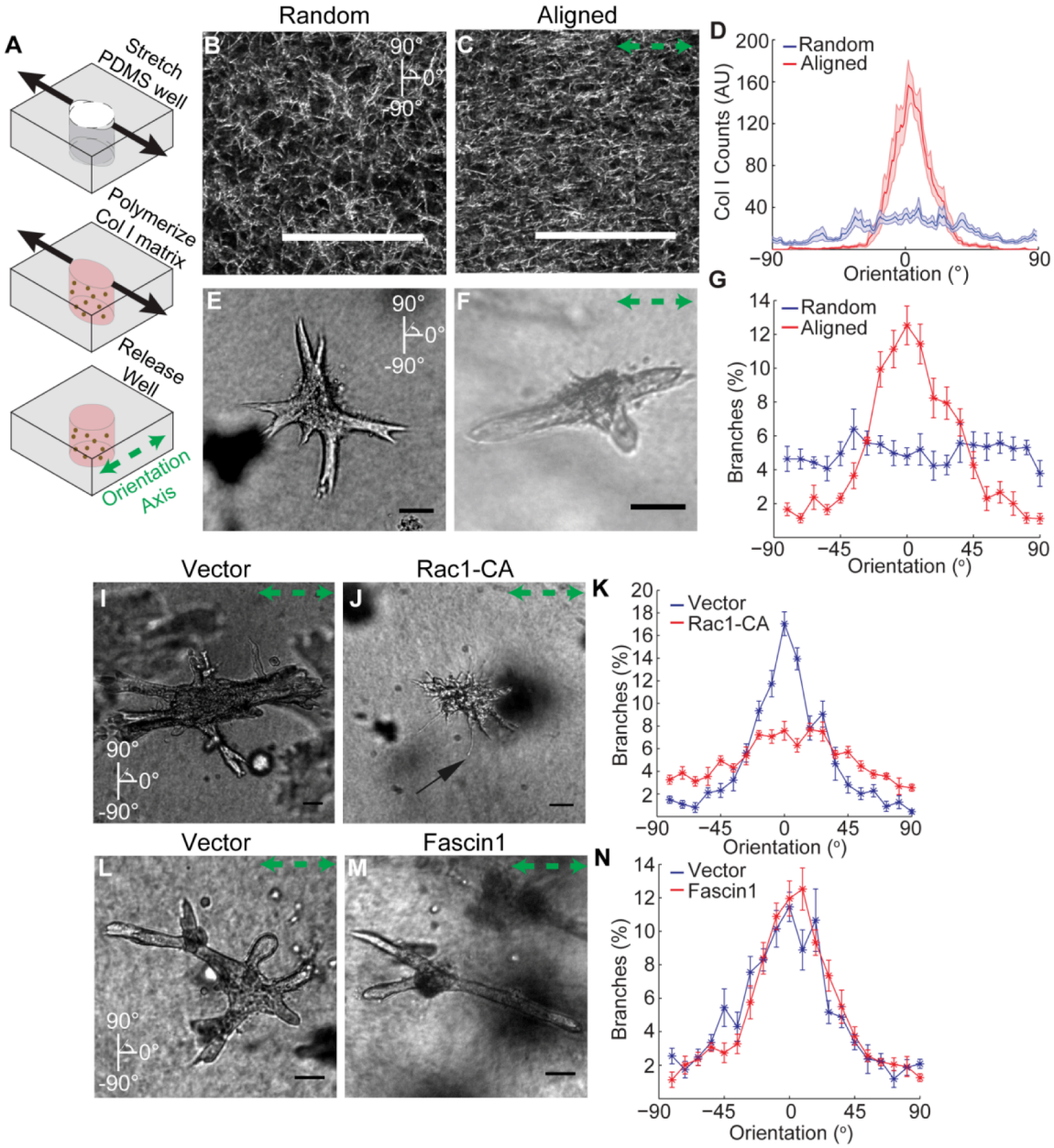

Figure 2-2: Epithelial cells follow Col I fiber orientation in a Rac1 dependent manner in culture. Method for axially orienting fibers within 3D Col I matrices (A). Confocal reflection of control (B) and oriented (C) Col I matrices with the orientation axis indicated (green arrows). Fiber alignment significantly increases upon compression (D); values are mean ± SEM, n=10 (matrices). Branching mammary explants in random (E) and oriented (F) Col I matrices. Quantification of branch orientation between explants in control versus oriented Col I matrices (G); mean ± SEM, n= 5-6. Compared to aggregates expressing vector alone (H), branch orientation of Rac1-CA expressing aggregates (I) was significantly disrupted (J); mean ± SEM, n= 5-6. When compared to aggregates with vector alone (K), fascin-1 overexpression had a modest, though not significant, enhancement in branch orientation (M); values are mean ± SEM, n= 5-6. Scale bar in (B,C,E,F,H,I K, L) represents 50µm.

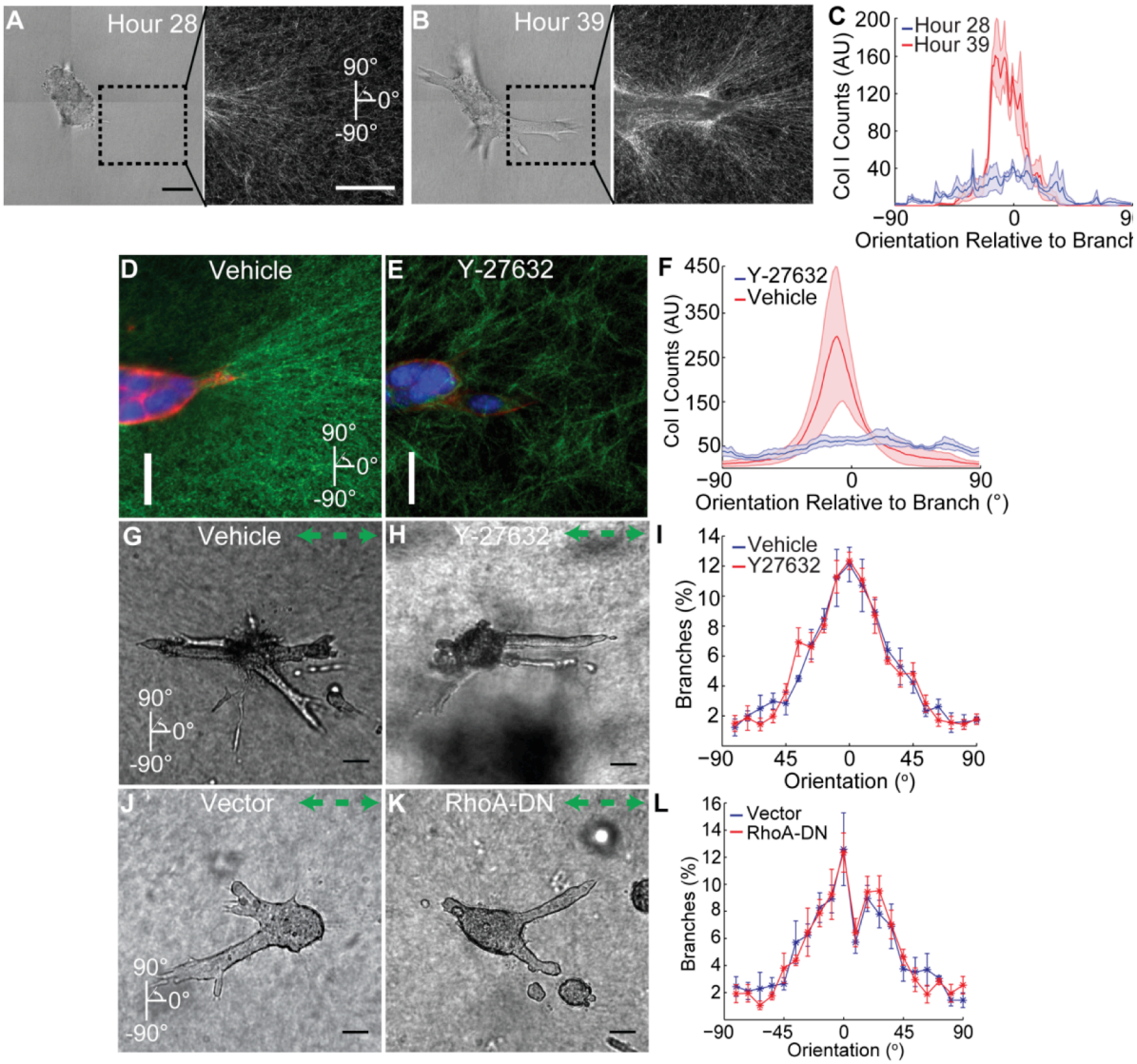

Figure 2-3: ROCK-dependent contractions are involved in generating, not sensing, Col I fiber orientation. Time-lapse microscopy of mammary explants (A-C). Representative explant at 28 (A) and 39 (B) hours, concurrent with early and late stage outgrowth. Confocal reflection of Col I proximal to a representative branch site (A, black inset) showed dramatic re-organization by 39 hours (B). Fiber orientation analysis at branch sites demonstrated a substantial increase in Col I co-orientation to branch direction by the late stage (C); mean ± SEM, n= 3 (branches). Representative branch sites from either vehicle (D) or Y-27632 treated (E, 20μM) aggregates, with Col I (green), DAPI (blue) and phalloidin (red) shown. Fiber orientation analysis found a loss of Col I co-orientation to branches upon ROCK inhibition (F); mean ± SEM, n=5. Col I orientation sensing was assessed by embedding aggregates in patterned matrices (G,H,J,K, green arrows). Branch orientation treated with vehicle alone (G) or Y-27632 (H) showed no difference in orientation (I); mean ± SEM, n=5. Quantification of aggregates expressing vector alone (J) versus RhoA-DN (K) found no significant difference in branch orientation (L); mean ± SEM, n=5. Scale bars in (A, D, E, F, G, H, J, K) represent 50μm.

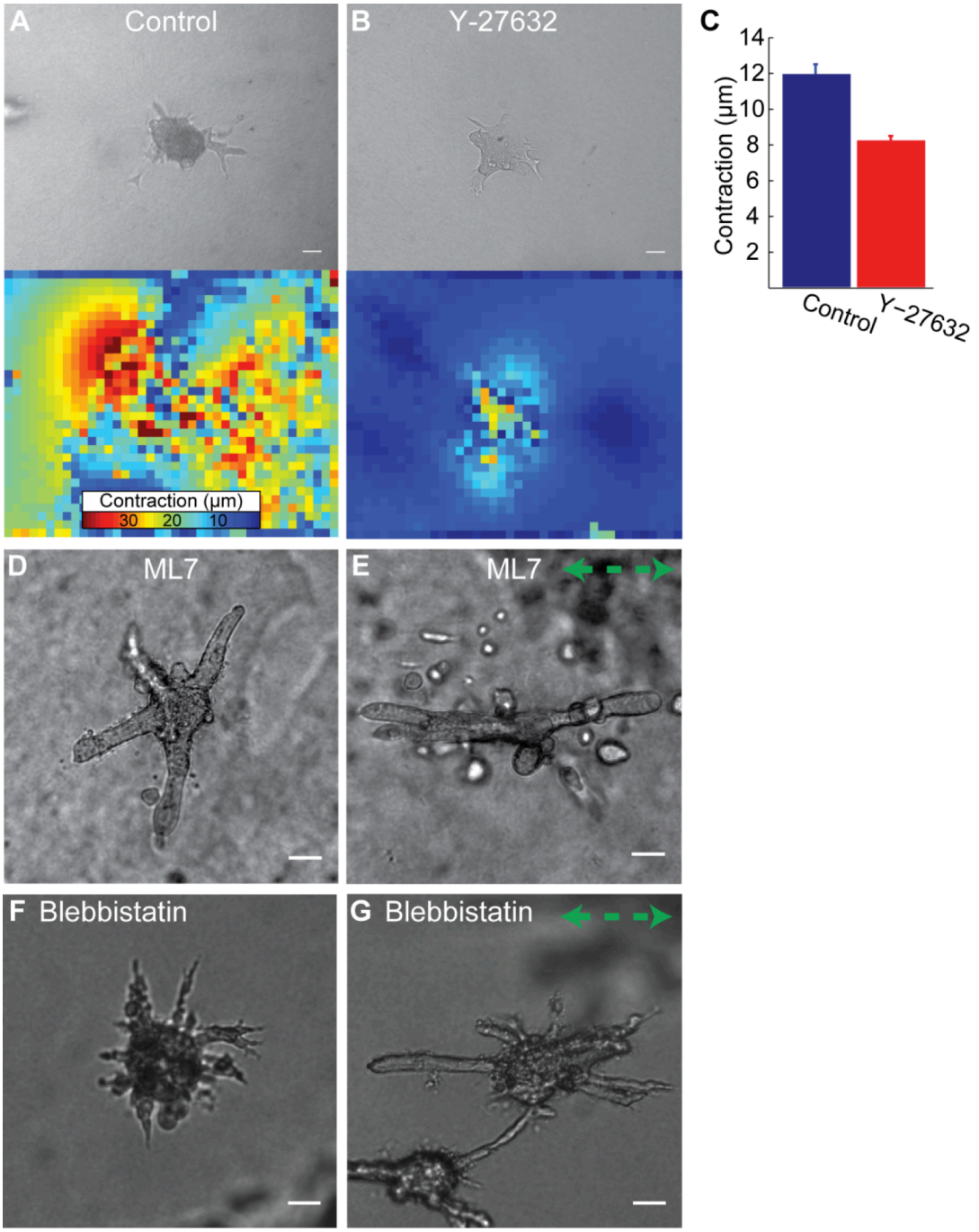

Figure 2-4: Time lapse studies of EpH4 aggregates untreated (A, upper) or in the presence of the ROCK inhibitor Y-27632 (B, 20μM). While untreated aggregates generate contractions (A, lower) during branching, contraction magnitude significantly decreases upon Y-27632 treatment (C); values are mean ± SEM, n=7,10. Inhibition of Myosin light-chain kinase with ML7 (1μM) in branching aggregates did not disrupt branching in control matrices (D) nor branch orientation in axially aligned matrices (E). Disruption of type II nonmuscle myosin affinity to actin by blebbistatin treatment (20μM) altered branching morphology in control matrices (F) but failed to disrupt branch oriented in axially oriented matrices (G). Scale bar in (A,B, D-G) represents 50μm.

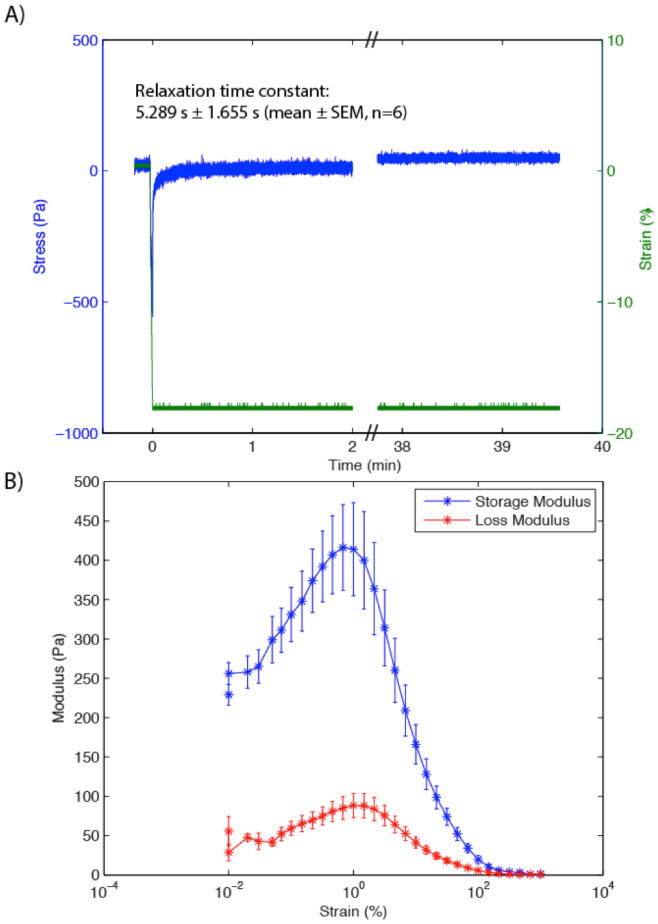

Figure 2-5: Collagen mechanical characterization. A) Representative collagen compression stress relaxation response. Collagen relaxes quickly relative to branching time scale. B) Collagen shear amplitude sweep. (Mean ± SEM, n=4)

Chapter 3: External forces can phenotypically revert malignant breast epithelial structures

With:
Mina J. Bissell[2]
Daniel A. Fletcher[1,4]
Walter Orellana[2,3]
Clay D. Reber[1]
Kandice Tanner[2,3]

[1] Department of Bioengineering, University of California, Berkeley, CA

[2] Life Sciences Division, Lawrence Berkeley National Laboratory, Berkeley, CA

[3] Center for Cancer Research, National Cancer Institute, National Institutes of Health,

Bethesda, MD

[4] Physical Biosciences Division, Lawrence Berkeley National Laboratory, Berkeley, CA

Abstract
Single breast epithelial cells embedded in three-dimensional laminin-rich extracellular matrix gels grow to form highly organized, growth-arrested acini. Malignant cells form larger, disorganized structures, but they can be 'phenotypically reverted' into acini by treatment with pharmacological reverting agents [36]. While extracellular matrix stiffness has been shown to be important in acinar morphogenesis [57], the role of external forces remains unclear. Here, we investigate the effects of external compression on acinar morphogenesis. Using an elastic chamber to apply a transient compressive force, we found that compressed malignant cells formed growth-arrested, polarized acini complete with lumen, rather than the disorganized structures observed in uncompressed gels. This 'phenotypic reversion' of malignant cells under compression occurred without the use of exogenous pharmacological agents, and resulted from compression applied at the one-cell stage, suggesting that early developmental steps are affected. Time-lapse microscopy of the malignant cells under compression revealed that external forces restore coherent rotation of the cells and lead to the formation of organized acini, which has been found to be critical for acinar development and lost in malignancy [75]. Blocking E-Cadherin function eliminated any compression sensitivity, indicating that cell-cell communication was required for force-induced reversion. Our findings suggest that external forces can mechanically reprogram malignant cells to re-enter the correct morphogenetic program.

Introduction

Acinar morphogenesis is the process by which epithelial cells form polarized, growth-arrested secretory components of glands. This process requires the coordination of many biochemical and biophysical cues, and the breakdown of these cues can promote malignancy, [30, 41]. In 3D culture, acinar morphogenesis can be modeled by embedding breast epithelial cells into a laminin-rich extracellular matrix. Normal epithelial cells grow into polarized, growth-arrested structures called acini [150, 151].

In contrast, malignant breast epithelial cells grown in 3D laminin-rich extracellular matrices form large, disorganized structures [36, 77]. Treating these malignant cells with various inhibitors can 'phenotypically revert' them into a structure resembling the normal cells [36, 152]. Even though these cells remain genetically malignant, manipulating the local biochemical environment can promote a non-malignant phenotype.

Mechanics also play an important role in acinar morphogenesis. Non-malignant mammary epithelial cells grown on very stiff substrates form malignant, non-polarized structures [57]. Increased stiffness is thought to allow for increased cell-generated contractile forces, leading to downstream signaling changes that promote malignancy. Disrupting cell-ECM interaction by blocking β1-integrin function reverts malignant cells to a phenotypically normal structure [36].

Contractile machinery also plays an important role in coherent angular motion seen in acinar morphogenesis of mammary epithelial cells [75]. Malignant cells – which do not form spherical structures – move randomly, whereas primary and non-malignant cells rotate together in a coherent fashion to form spherical structures. This cell-generated rotation is important for acinar morphogenesis, as disrupting rotation prevents the cells from assembling into a spherical tissue structure. Interestingly, malignant cells treated with phenotypic reverting agents display restored coherent angular motion [75]. Taken together, these experiments demonstrate that cell-generated forces such as coherent angular motion and cell-ECM traction dramatically influence multicellular epithelial structure. However, the effect of externally applied forces on acinar morphogenesis remains unclear.

Externally applied compression dramatically alters the structure and behavior of many tissues and cells. For example, step compression of whole cartilage tissue increases interleukin expression [153] and dynamic compression of bone has long been known to enhance bone remodeling [154]. Sensitivity to external forces is not limited to musculoskeletal tissue. Elastic compression jackets are a common treatment to prevent scar tissue formation in burn injuries [155], partly by inhibiting fibroblast cytokine secretion and increasing apoptosis [156]. In rat models, chronic nerve compression increases both apoptosis and proliferation [106]. Compressing tumor spheroids in agarose gels also increases apoptosis, but inhibits proliferation [72, 73]. In 2D wound assays, compression alters the motility of both malignant and non-malignant breast epithelial cells

[71], indicating that external compressive forces may alter multicellular mechanical processes like collective cell migration.

Given the dynamic mechanical processes involved in acinar morphogenesis and tumorigenesis, we hypothesized that external compression could affect the formation of a multicellular epithelial structure. In this study, we applied single short-timescale step compressive stresses to malignant breast epithelial cells cultured in laminin-rich ECM over long timescales. Compressed single cells grew into smaller colonies that better resembled healthy acini. Compression did not directly inhibit growth, but rather encouraged coherent rotation of malignant cells doublets, allowing them to form acinar structures.

Results

The HMT3522 human breast epithelial cancer cell progression is a model system for understanding acinar morphogenesis and tumor growth. Non-malignant HMT3522-S1 cells grow into organized acini when embedded in laminin-rich extracellular matrix (Figure 3-1A) [150, 151]. In contrast, malignant HMT3522-T4-2 cells grow into disorganized structures (Figure 3-1A) [36, 77]. Malignant T4-2 cells can be treated with pharmacological compounds to 'phenotypically revert' them into organized structures resembling the non-malignant acini (Figure 3-1A) [36, 152]. Among other factors, this model system has been used to demonstrate the importance of matrix stiffness [57] and cell-matrix interaction [36] in acinar morphogenesis.

Given the importance of matrix stiffness and integrin activity, we hypothesized that external forces could play a role in 'phenotypic reversion' of malignant breast epithelial cells. To test this hypothesis, we embedded single malignant T4-2 breast epithelial cells in laminin-rich extracellular matrix as previously described [37], and polymerized the matrix in deformable elastic wells (Figure 3-1B, inset). Thirty minutes after polymerization, we applied a step displacement to the well (23% compressive strain) and observed colony growth over 10 days later.

We grew non-malignant S1 and malignant T4-2 cells in our silicone wells without compression to ensure that our assay replicated previously reported differences in colony growth from commercial well plates [36]. Without compression, malignant T4-2 cells grew into significantly larger colonies than non-malignant S1 cells (Figure 3-1C, $p=0.007$), consistent with the previous results. This allowed us to compare compressed malignant T4-2 colonies to both non-malignant S1 and malignant T4-2 uncompressed controls. Compression of malignant T4-2 cells led to a significant reduction in colony size ($p=0.009$). Compression sufficiently reduced colony growth to the point that these colonies were not detectably different in size from non-malignant S1 acini ($p=0.361$).

Some types of extracellular matrix gels strain-stiffen in the strain regimes of interest here [157]. Increases in stiffness are sufficient to cause non-malignant breast epithelial cells to grow into disordered colonies [57]. Therefore, it was important to determine whether or not applied strain led to changes in mechanical properties of laminin-rich extracellular matrix. Using a parallel plate rheometer, we measured the storage and loss moduli of

laminin-rich extracellular matrix for shear strains from 0.01% to 1000% (Figure S1A). Laminin-rich extracellular matrix did not detectably deviate from linear elastic behavior as measured by storage or loss moduli from 0.01% to 22% strain (p=0.805, 0.454), approximately the range of interest in our experiments. This is consistent with previously reported mechanical behavior [158]. Responses to applied compression in our system are therefore unlikely to be due to external-force-driven changes in mechanical properties of the ECM.

We next investigated whether compression-induced changes to colony size were dose-dependent. Changing amount of step displacement on the deformable wells allowed for applied compressive strains from 0-23% (Figure 3-2A). Compression resulted in approximately a 25% decrease in colony cross-sectional area for all tested strains above 15% (Figure 3-2B). In contrast, 10% compressive strain did not result in a detectable difference in colony size. Confocal microscopy confirmed that compressed colonies had significantly fewer cells (Figure 3-2C, p=0.012).

In addition to decreased colony size, full 'phenotypic reversion' requires growth arrest and improvement in structure. Non-malignant S1 cells exit cell cycle at late stages of acinar morphogenesis as measured by absence of Ki67 – a protein found in all stages of cell cycle [35]. Ki67 immunofluorescence demonstrated compression-induced growth arrest of malignant T4-2 colonies (Figure 3-2D, p=0.004).

In conjunction with growth arrest, non-malignant acini exhibit multicellular organization into polarized structures. Because this improved organization is required for growth arrest in non-malignant cells [89], we investigated the effects of compression on the formation of multicellular acinar structures. We quantified multicellular structure in binary fashion by measuring the frequency of formation of E-cadherin 'star' patterns or lumens. Compression enhances the formation of e-cadherin 'star' patterns (Figure 3-3A-B, p=0.015) and lumen formation (Figure 3-3C-D, p=0.0002). This suggests that external compression can 'phenotypically revert' malignant T4-2 cells.

Compression did not directly inhibit proliferation, but still improved acinar structure by enhancing growth arrest and organizing structure formation. Compression could reduce colony size in two different ways: directly slowing proliferation or eventually inducing growth arrest. Non-malignant S1 colonies exhibit growth arrest [151], but also undergo first mitosis later than malignant T4-2 cells [75]. Adding pharmacological reverting agents to T4-2 cells slowed the time of first mitosis to match that of the S1 cells [75]. In contrast, time-lapse microscopy of compressed malignant T4-2 cells did not show a detectable difference in the time of first mitosis (Figure 3-S2, p=0.68). This suggests that even though compressed colonies are smaller, this effect is not due to direct mechanical inhibition of proliferation.

Importantly, our compressive stress relaxation tests of laminin-rich extracellular matrix demonstrated that stress relaxes to zero on relatively fast time scales (Figure 3-S1B, relaxation time constant 66s ± 16s, mean ± standard error). Stress relaxation occurred on

time scales much faster than key processes in acinar morphogenesis, including first cell division (~12 hours), and growth arrest (~8 days). As a result, we hypothesized that compression changed early morphogenetic events, leading to phenotypic reversion.

An important factor in early phases of acinar morphogenesis is coherent rotation. Non-malignant S1 cells require coherent rotation to form spherical acinar structures, a process which requires several physical processes such as contractility and actin polarity [75]. Given the dynamic mechanical nature of this process, we investigated whether compression could restore coherent rotation of malignant cells. Using time-lapse microscopy, we observed that compression improves the rotation of malignant single cells (Figure 3-4A, Movie M1 and M2). Compression leads to a restoration of coherent rotation of malignant T4-2 cell doublets (Figure 3-4B, $p=0.009$).

In non-malignant S1 cells, blocking E-cadherin function disrupts coherent rotation of cell doublets [75] while disrupting structure formation [89]. If the mechanism by which compression phenotypically reverted cells was primarily by enhancing coherent rotation of malignant cells, disrupting cell-cell communication should eliminate the effects of compression. We treated malignant T4-2 cells with function-blocking E-cadherin antibody [159] before compression (Figure 3-5A). Once E-cadherin function was blocked, colonies did not grow smaller in response to compression (Figure 3-5B, $p=0.94$). In contrast, malignant T4-2 cells treated with IgG control antibody still responded to compression (Figure 3-5B, $p=0.05$). This evidence suggests that external compression induces phenotypic reversion by encouraging malignant cells to re-enter the correct morphogenetic program.

Discussion

We report that a transient compression applied to single malignant breast epithelial cells less than an hour into growth significantly decreased colony size over the course of a week or more. This effect of compression was dose-dependent, with lower strains leading to less decrease in colony size. Growth inhibition of compressed cells was associated with improved structure, similar to phenotypic changes observed with chemical 'reverting agents' such as function-blocking B1-integrin antibody, EGFR inhibitor, PI3-Kinase inhibitor, and MAP-Kinase inhibitor [36, 46]. Like treatment of cells with these reverting agents [160], compression pushed cells towards a nonmalignant phenotype. While previous studies of tumor mechanics in 3D suggest that matrix stiffness can affect growth and structure formation [57], the strain range used in this study did not decrease stiffness of the matrix, but still led to a decrease in malignancy.

Sustained compression inhibited growth of multicellular tumor spheroids embedded in agarose by altering proliferation and apoptosis rates [73]. This is unlikely to be the mechanism by which phenotypic reversion occurs in our assay, as the time to first mitosis did not noticeably change in our experiments. Additionally, the stress we applied was transient, completely relaxing in less than an hour. At first glance, it seems surprising that cells exhibit a phenotypic difference 10 days after a short-term force input. However, previous work suggests that controlled colony growth from a single cell is different from

pre-aggregated cluster growth. Colonies formed with pre-aggregated non-malignant cells neither coherently rotate nor form growth-arrested acini [75]. This suggests that cell-cell junctions formed during coordinated mitosis are somehow different than those formed by pre-aggregating cells. Our E-cadherin function blocking experiments suggest that compression promotes 'normal' cell-cell junction formation in malignant single cells.

Transiently compressing single malignant cells could help establish polarity and coordinated growth. Compression increases the frequency of coherent rotation, a process previously associated with the formation of a phenotypically normal structure [75]. Previously, coherent rotation at the two-cell stage has been associated with formation of a leading edge of actin in the single cell [75]. These results suggest that additional investigation of the mechanics of polarity formation could provide important insight into development and tumorigenesis.

Our finding that externally applied forces can cause cells to form less malignant structures could also be important for functional differentiation. Functional differentiation of mammary epithelia for milk production *in vivo* requires attachment to laminin-rich basement membrane [161], a process that requires integrin signaling [38, 39]. In addition to proper ECM ligand presentation, milk production requires the ECM to be the correct stiffness. Single mammary epithelial cells grown on matrices mimicking the stiffness of mammary tissue produce more β-casein than cells grown on very stiff matrices [42]. Taken together with the results presented here, this motivates further work investigating the role of external forces in milk production.

Methods

Cell Culture

Culture of non-malignant HMT3522-S1 and malignant HMT3522-T4-2 cells was performed as previously described [37, 77, 150, 151]. Briefly, cells were cultured on collagen I-coated tissue culture flasks until embedded in laminin-rich extracellular matrix. Cells in 2D and 3D were cultured in a 1:1 mix of Dulbecco's Modified Eagle's Medium and Ham's F-12 (UCSF Cell Culture Facility). Medium contained insulin, transferrin, sodium selenite, β-estradiol, hydrocortisone and prolactin. Media for S1 cells also contained epidermal growth factor. The laminin-rich extracellular matrix was Matrigel™ lots A7750, 04147, 36819, with protein concentration ranging from 9.2 to 9.4 mg/mL (BD Biosciences).

E-cadherin function blocking was performed as previously described [75, 89]. Cells were gently centrifuged and resuspended in a solution of mouse anti-E-Cadherin (Invitrogen 13-1700). This solution was mixed and resuspended in laminin-rich extracellular matrix. The final E-cadherin antibody concentration was 200μg/mL. Control experiments were performed with a mouse IgG control antibody (BD Pharmingen 555749).

Compression

After embedding cells, extracellular matrix gels were compressed in custom stretchable wells made of poly-dimethylsiloxane, similar to our previous work (Chapter 2). Wells were made of Sylgaard 184 (Dow Corning) polymerized at a 9.5:1 ratio of base to curing agent.

This mixture was poured into custom-made laser-cut acrylic molds and polymerized at 60C overnight (laser cutter: ULS2.0 Engraver, clear cast acrylic: McMaster-Carr). Silicone wells were cleaned under ultraviolet light for seven minutes, washed in distilled, deionized water for at least four days under gentle vacuum, and then washed with the cell culture media (without additives) at 37C for another four days before use.

Immediately prior to use, wells were stretched using custom-made laser-cut acrylic frames and stainless steel dowel pins (McMaster-Carr). Cell-embedded matrix (200μL) was poured into the stretched well and polymerized at 37C, 5% carbon dioxide (Figure 3-1B). After 30 minutes of polymerization, the stainless steel dowel rods were removed with pliers to apply a step compression to the matrix. Media was added, and the wells were returned to the incubator. Media was changed every other day during growth. Each compressed gel had a matched uncompressed control gel made with the same cell-matrix mixture.

Applied strain was varied by changing the amount of initial stretch applied to the well before compression. Strain ranged from 0-23% compression as measured by photographs of the stretched wells.

Immunofluorescence

Colonies were fixed and stained as previously described [37] after ten days of growth. Media was aspirated away and the cell-matrix mixture was directly smeared onto glass microscope slides. These smears were briefly dried at room temperature, but not completely dried out (~20 minutes). Smears were then fixed in 4% paraformaldehyde in phosphate-buffered saline for 30 minutes and washed with phosphate-buffered saline for 10 minutes. Cell membranes were then premeabilized in 0.5% Triton X-100 (in distilled, deionized water) for 30 minutes before 1 hour blocking with 3% bovine serum albumin (in phosphate-buffered saline). Primary antibodies were incubated overnight at 4C in the same blocking solution. Cultures were then washed with phosphate-buffered saline two times (10 minutes/wash). Hoechst and secondary antibodies were incubated in blocking solution for 2 hours, and cultures were washed with phosphate buffered saline three more times. The samples were mounted on cover slips with ProLong Gold Anti-fade reagent (Invitrogen).

Primary antibodies used were mouse anti-human E-cadherin (1:500,BD Biosciences 610182) and rabbit anti-human Ki67 (1:400, Vector VP-K451). Secondary antibodies used were Alexa 488 and Alexa 568 anti-mouse, anti-rat, and anti-rabbit (all 1:250, Invitrogen). DNA was stained with Hoechst during secondary antibody incubation.

Microscopy and image analysis

Brightfield microscopy for colony size measurements

After 10 days of growth, colonies were imaged directly in the wells with a 10x objective on a Zeiss Axiovert 200. Fifty fields of view were taken for each gel to measure colony size. Colony size was measured by tracing projected colony area in ImageJ (National Institutes for Health). Researchers taking measurements were blinded as to whether samples were compressed in order to prevent measurement bias. For each gel, an average colony size

was measured and compared to the matched control. For initial compression experiments, 2-tailed, paired t-tests were used to compare mean area. For dose-dependent experiments, statistical significance was measured using a 2-tailed paired analysis of variance with multiple comparison test. For E-cadherin experiments, 1-tailed paired t-tests were used to see if antibodies prevented compression-induced reduction in colony size.

Immunofluorescence imaging for cell counts, fluorescent labels

Confocal immunofluorescence images were taken with a 20x oil-immersion objective on a Zeiss 710 laser-scanning confocal microscope. Multichannel image stacks were acquired for each colony labeled nuclei and fluorescent proteins of interest. Cell count was measured by counting labeled nuclei using thresholding and watershedding methods in ImageJ (modified from count_3D_nuclei_v2.txt by Vytas Bindokas, Univ of Chicago). Presence of Ki67, lumen, and E-cadherin structure was measured manually in blinded fashion.

Time-lapse microscopy and analysis

Time-lapse microscopy was performed in a custom-built microscope inside a cell culture incubator. This microscope used an electrically shuttered green LED (Phillips Luxeon Rebel), a CMOS camera (DCC1545M, Thorlabs), and a 10x 0.25NA objective (Nikon) to perform brightfield microscopy. An encoded XY stage and a motorized z-focusing mechanism (Prior Scientific) were used to take measurements at multiple positions simultaneously. After compression, gels were placed in a custom-made 3D-printed ABS plastic holder and put into the time-lapse microscope. The system took approximately 1 hour to equilibrate, and then images were taken at every 10 minutes. Time-lapse microscopy was stopped after 50 hours. Blinded observers measured the time to first cell division and rotation direction of single cells and doublets. In each separate experiment, at least 5 fields of view and a minimum of 50 cells in total were measured for each condition.

Mechanical testing

Stress relaxation tests were performed on an Electroforce 3200 (Bose) using a 50g load cell (Honeywell Sensotec) and custom made 1" cylindrical aluminum compression platens. The lower compression platen was pre-heated to 37C using feedback-controlled thermistors and resistive heating elements (Warner Instruments TC-324B, 64-0106, 64-0274 RH-2). The distance between the upper and lower compression platen was calibrated after pre-heating for 30 minutes. A droplet of Matrigel™ (100μL) was placed on the pre-heated lower platen, and the upper platen was immediately brought down to contact the Matrigel™ droplet. Space between the platens was held at 0.4 mm, and the gel was allowed to polymerize for 30 minutes. This led to formation of a 0.4 mm tall gel with cross-sectional area of 250 mm^2. Compression was applied at a rate of 0.05 mm/s for deformation of 0.04 mm (10% strain). Strain rates were chosen to approximately mimic strain rates in the stretchable wells. Load was measured for 40 minutes, by which time a residual load could not be measured. Relaxation time constants were measured by measuring the amount of time to reach five time constants worth of decay from peak stress (99.4% decay).

Storage and loss moduli were measured by taking shear amplitude sweeps on a parallel plate rheometer (Anton Paar MCR302). The testing environment consisted of a quartz lower plate and a 8 mm diameter stainless steel upper plate. Plates were pre-heated to 37C

and humidified using a water jacket-heated environmental chamber. Matrigel™ was polymerized in similar fashion to stress relaxation tests, except that gels 0.4mm tall and 200 mm^2. Storage and loss moduli were measured from 0.01%-1000% shear strain. This strain regime was chosen to ensure that material breakdown occurred and was measurable. Moduli at 0.01% and 21.5% strain were compared using a 2-sided t-test to determine if material properties changed in the regime of interest.

Acknowledgements
We would like to thank the Fletcher and Bissell Labs for their helpful comments and advice. Professor Sanjay Kumar generously allowed use of his rheometer. The Bose Electroforce machine was part of the California Institute for Regenerative Medicine Shared Laboratory at UC Berkeley.

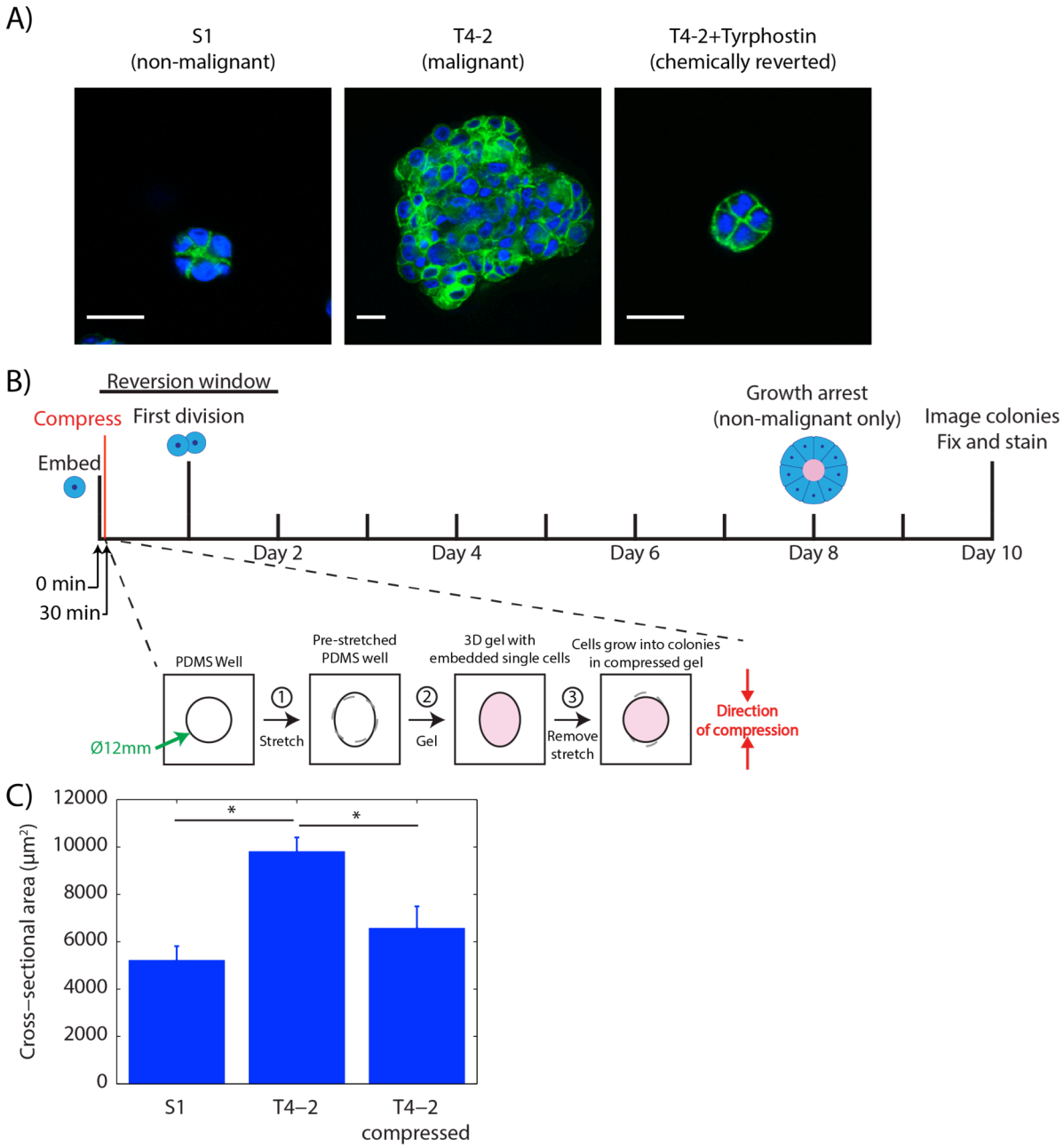

Figure 3-1: Compression inhibits colony growth. A) Representative images of S1 and T4-2 growth. Scale bars 25μm. B) Cells were compressed after 30 minutes of polymerization at 37C, long before first division (Day 1) or formation of growth-arrested colonies. C) 23% compression of malignant colonies leads to reduction in colony size. * p<0.05. (N=3, 11 and 5 gels)

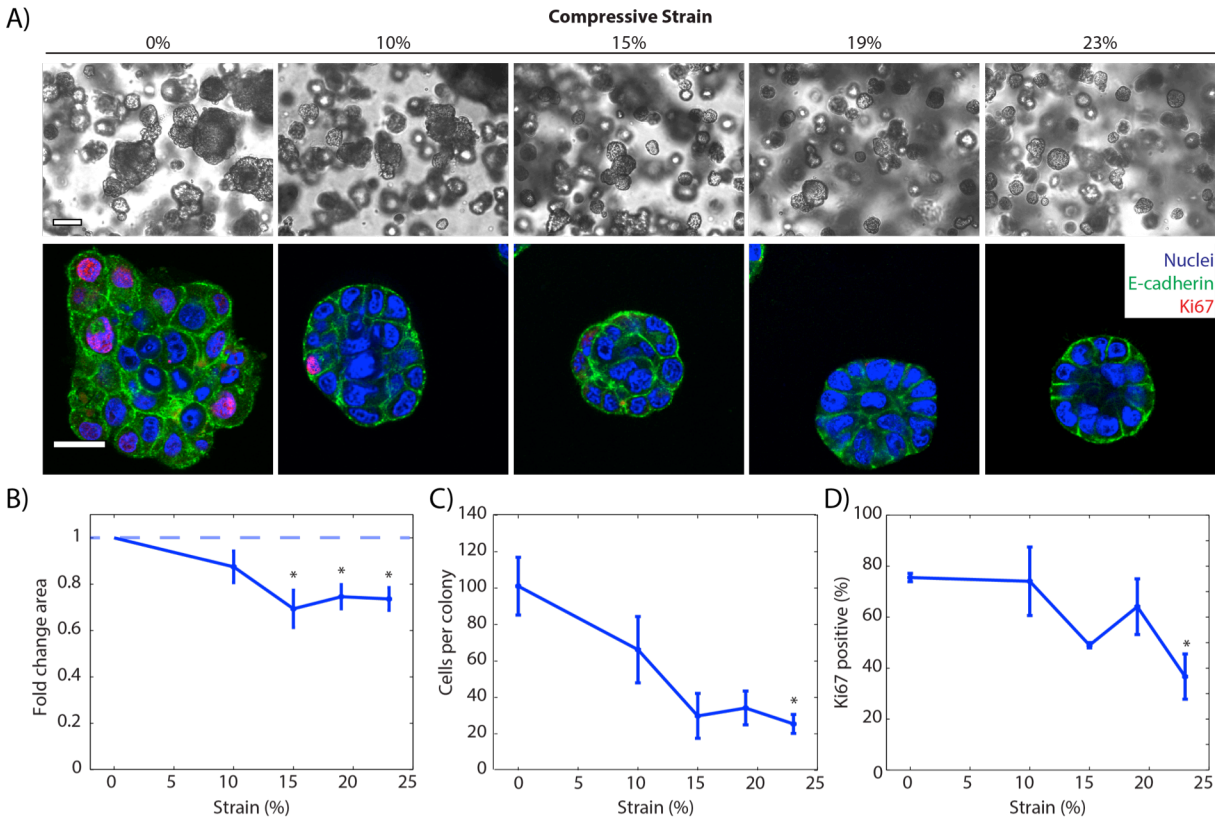

Figure 3-2: Compression inhibits malignant cell colony growth in a dose-dependent fashion. A) Brightfield and confocal immunofluorescence images of breast epithelial cell colonies grown in compressed gels. Scale bars: 100µm brightfield and 25µm confocal. B-D) Colonies grown in compressed matrices are smaller, have fewer cells, and are growth arrested. *p<0.05. For (B), n=4,4,7, and 6 gels. For (C-D), n=11,3,3,2, and 4 gels.

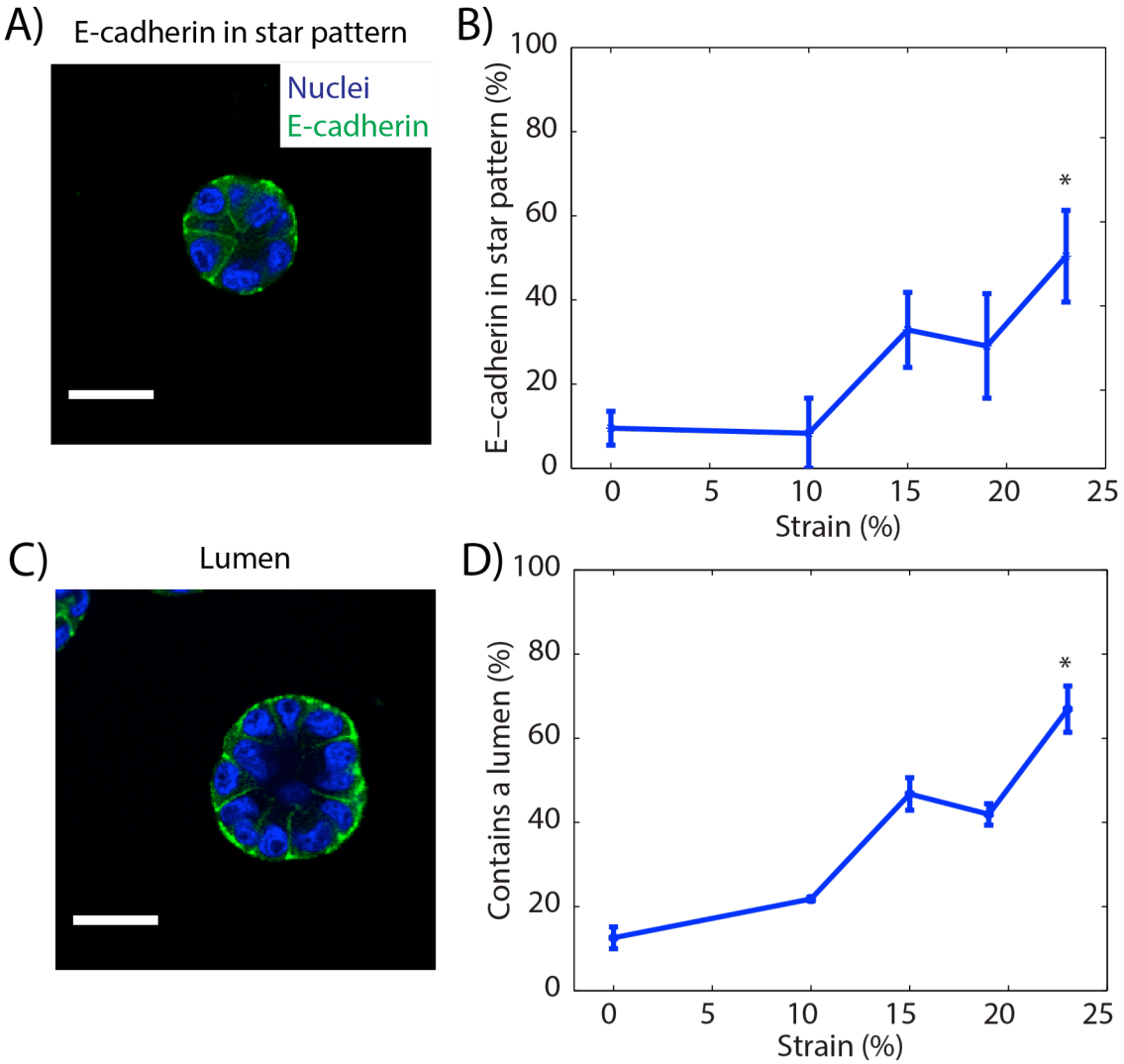

Figure 3-3: Compression improves colony structure. A) Confocal immunofluorescence image of a compressed colony with e-cadherin in a star pattern. Scale bar 25µm. B) Compression increases the frequency of e-cadherin found in a star pattern (n=11,3,3,2, and 4 gels). C) Confocal immunofluorescence image of a compressed colony with a lumen forming. D) Compression increases the frequency of lumen formation (n=11,3,3,2, and 4 gels). *p<0.05 (multiple comparison).

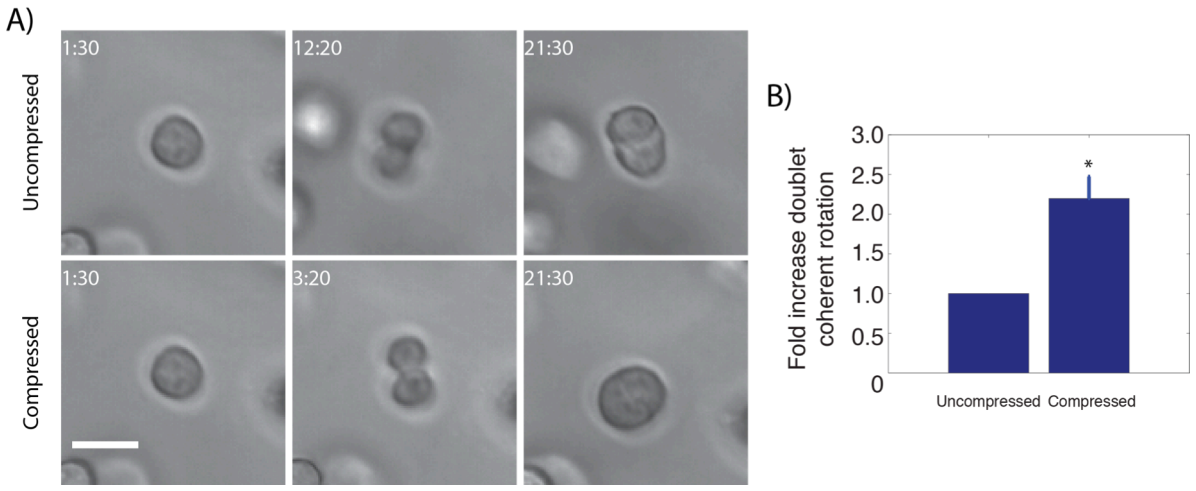

Figure 3-4: Compression restores coherent rotation of cell doublets. A) Time series of malignant T4-2 cells growing in uncompressed and compressed matrices. Scale bar 25µm, time in h:mm. See supplementary movies M1 and M2. B) Cells at the two-cell stage rotate more coherently in compressed matrices. Mean ± SEM. N=4 gels. *p<0.01.

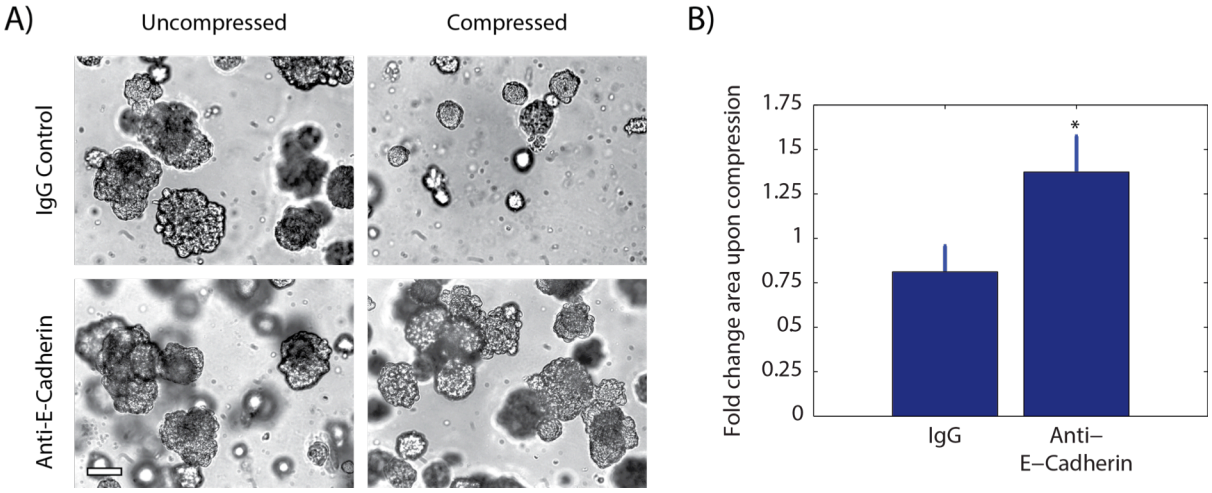

Figure 3-5: E-cadherin function is required to sense compression. A) Brightfield images of colonies treated with function-blocking E-cadherin antibodies or control. Scale bar 100µm. B) Blocking E-cadherin prevents compression-induced reduction in colony size (N=2, 2 gels).

Supporting Information

Movie M1: Time-lapse of uncompressed malignant breast epithelial cells - Scale Bar 25µm

Movie M2: Time-lapse of compressed malignant breast epithelial cells - Scale Bar 25um

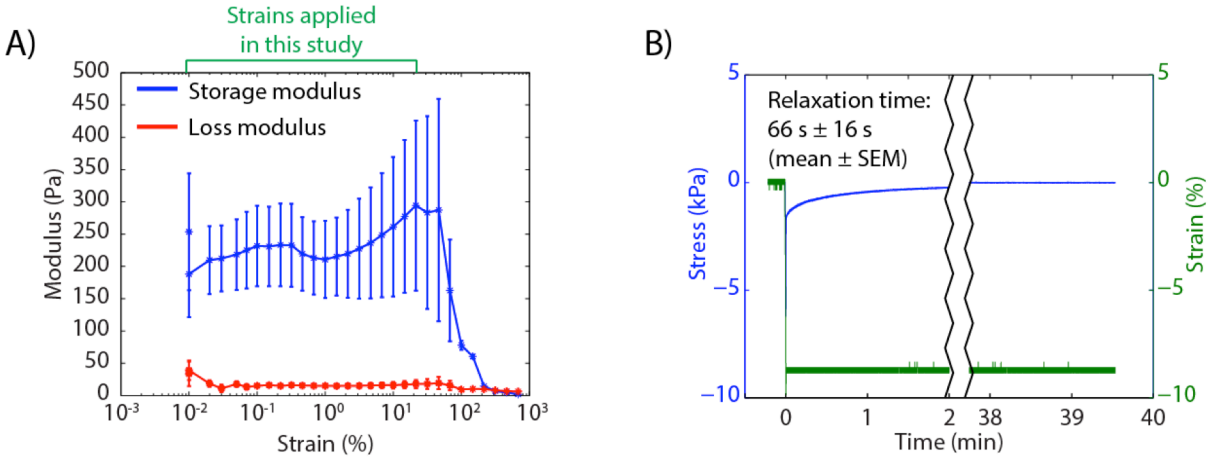

Figure 3-S1: Laminin-rich ECM mechanics. A) Shear rheometry data showing that laminin-rich ECM gels do not significantly stress stiffen or soften under strains applied in this study (0-23%) (n=5 gels). B) Representative stress relaxation of laminin-rich ECM gel under compression. Gels stress relax to zero stress with a characteristic time constant on the minute scale, much shorter than division (n=4 gels).

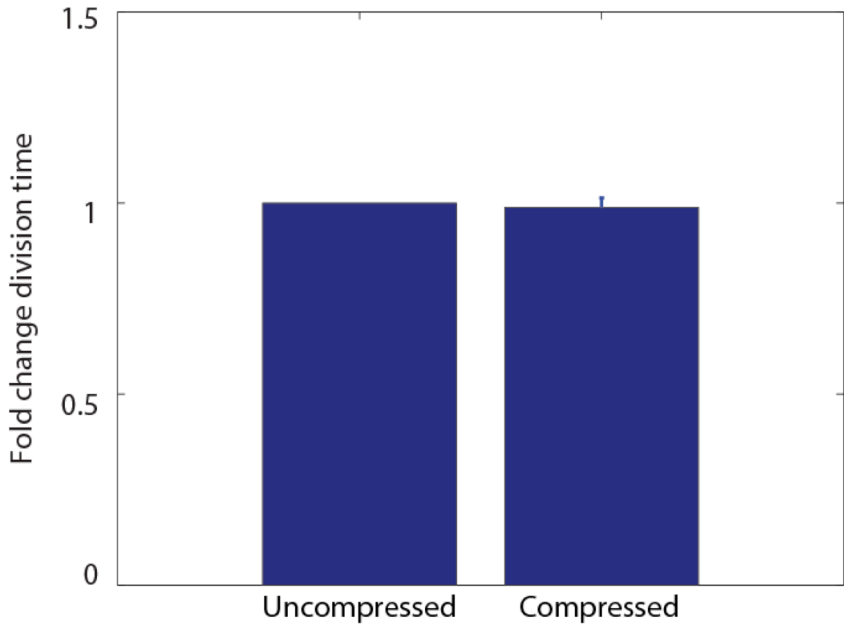

Figure 3-S2: Time to first division does not detectably change in response to compression for malignant cells.

Chapter 4: Multicellular architecture of breast epithelia influences mechanics of the epithelial structure

With:
David B. Camarillo[2]
Hana El-Samad[2]
Daniel A. Fletcher[1,4]
Clay D. Reber[1]
Chris H. Rycroft[3]
James A. Sethian[3]
Kevin D. Webster[4]
Valerie M. Weaver[5]

[1] Department of Bioengineering, University of California-Berkeley, Berkeley, CA

[2] Department of Biochemistry and Biophysics, University of California-San Francisco, San Francisco, CA

[3] Department of Mathematics, University of California-Berkeley, Berkeley, CA

[4] Biophysics Program, University of California-Berkeley, Berkeley, CA

[5] Department of Surgery, University of California-San Francisco, San Francisco, CA

Abstract
During breast carcinoma progression, epithelial cells often grow into the lumen and form a filled structure. Breast cancers are often stiffer than healthy tissue, and breast epithelial cells grow into abnormal, filled structures in response to matrix stiffness. Cell-matrix interactions have been an area of extensive study, and a growing body of work indicates that cell-matrix 'mechanosensing' is an important player in many cellular processes. Recent evidence suggests that epithelial cells also mechanosense through their cell-cell junctions, but it remains unclear how this interaction changes as a result of changes to multicellular structure during cancer progression. In this study, we investigated the role of multicellular structure on mechanical properties of the epithelial subunit. We extracted multicellular breast epithelial structures from laminin-rich extracellular matrix and performed creep compression tests on the structures. We found that hollow (MCF10A) structures were significantly more compliant than filled (MCF10AT) ones. This difference was found to be dependent on acinar structure, as neither single cells nor multicellular structures tested before lumen formation exhibited these differences. To further investigate the role of multicellular structure, we developed a multiphase simulation framework using the level set method to track displacements. Our model suggested a 3-fold increase in stiffness due to the lumen filling with cells, consistent with the 1.6-fold increase observed in experiment. We then used this model to simulate a single contracting cell in different multicellular structures. Using the forces and displacements from this single cell contraction simulation, we predicted the "perceived stiffness" of a single contracting cell as the lumen fills with cells. Based on this model, lumen filling could contribute approximately a 15% increase in the "perceived stiffness" of a single contracting cell independent of any changes to matrix mechanics.

Introduction

Physical forces drive many multicellular processes such as morphogenesis [75] and tumor growth [73]. Forces either originate from cells themselves, or can be applied externally to the tissue. Forces transmit through a tissue to single cells via direct attachment to other cells [68], adhesion to the extracellular matrix (ECM) [162], or the shearing force of fluid flow [69]. One important determinant of this force transmission is the mechanics of the cellular microenvironment. Previous studies extensively characterized the structure-mechanics relationship in ECMs (for example [63]) and showed that changes to ECM mechanical properties affect active cellular processes such as contraction [100], stem-cell differentiation [53], and growth signaling [163]. In mammary epithelial cells, milk production requires the appropriate ECM stiffness [42]. At the multicellular level, disruptions to ECM mechanics scale up to disrupt normal mammary epithelial tissue structure and growth [57] and contribute to malignancy [4].

In addition to the ECM, epithelial cells reside in a multicellular configuration where they are tightly attached to several other cells (Figure 4-1A). These connections are essential for proper development [89, 159] and function [164] of the tissue. Multicellular structure often changes during mammary ductal carcinoma progression as the lumen fills with cells (e.g., ductal carcinoma in situ [165]), but it remains unclear how these structural changes are associated with changes in multicellular mechanics or cell-cell forces. Epithelial cells have been shown to mechanosense through their cell-cell contacts [109], and increases in cell-ECM forces have been correlated to increases in cell-cell forces using traction force microscopy [68]. Taken together, these data suggest that nanonewton scale forces play essential roles in cancer and development, but we do not know whether multicellular architectural changes like lumen filling contribute to changes in cellular mechanosensing.

Single cell experiments suggest a mechanical difference between non-malignant and malignant mammary epithelial cells spread on a glass surface [166], but we do not yet fully understand the roles of multicellularity and biologically-relevant ECM on cell and tissue mechanics. Multicellular atomic force microscope (AFM) experiments characterized the elasticity of healthy mouse mammary organoids on a laminin-rich ECM gel [42]. Recently micropipette aspiration has been used to apply step forces to multicellular structures and study their time-dependent response. Xenopus laevis embryonic tissue behaves in a linear viscoelastic fashion [167] while murine sarcoma model tissues behave like a string of Kelvin-Voigt elements [116]. However, an investigation of how multicellular mechanics differs in phenotypically normal (hollow lumen) and pre-malignant (filled lumen) epithelia has not been performed.

To investigate differences in the mechanics of phenotypically normal and pre-malignant structures, we carried out *in situ* experiments using MCF10A (non-malignant) and MCF10AT (pre-malignant) mammary epithelial cells. We cultured MCF10A and MCF10AT cells long-term embedded within a laminin-rich ECM, extracted multicellular structures, and performed creep compression tests using an AFM (Figure 4-1B). The filled structures formed by MCF10AT cells were less compliant (stiffer) than hollow structures formed by

MCF10A cells. To study how changes in multicellular structure influence bulk multicellular elasticity, we developed a three-dimensional mechanical simulation of an acinus and calibrated it using our experimental creep data. Our simulation predicts that lumen filling would lead to decreased compliance consistent with the experimental results. Further simulations of single cell contraction within a hollow or filled structure predict approximately a 15% increase in perceived stiffness of single cells in a filled structure, suggesting an architectural reinforcement of the stiffening, possibly amplifying the tumorigenic mechanical signaling.

Results

Healthy and pre-malignant epithelial structures have different mechanical properties

We measured the mechanics of healthy and pre-malignant epithelial structures using the MCF10A and MCF10AT model system. MCF10A cells are a human-derived breast epithelial cell line [168]. When embedded in laminin-rich ECM, MCF10A single cells grow into large, structures with lumens after a period of 2-3 weeks (Figure 4-2A, [34]). In contrast, c-Ha-Ras transformed MCF10AT cells [80, 81] do not form lumens (Figure 4-2B, [82]). The MCF10A cell line has been used to demonstrate mechanical sensitivity of breast epithelial cells in the context of acinar morphogenesis [57] and growth factor sensitivity [163].

Because mechanosensitive breast epithelial cells form filled lumen structures in response to both genetic mutations [82] and increased matrix stiffness [57], we hypothesized that healthy and pre-malignant structures could have different mechanical properties, which might provide a mechanical reinforcement of pre-malignancy. Given recent evidence that cell-cell junctions are mechanosensitive [109], the mechanics of the whole multicellular structure could play an important role in tumor formation. We developed an extraction protocol that allowed us to extract cells from a laminin-rich ECM without protease digestion, allowing us to extract cells and colonies without cleaving structurally important proteins such as integrins and cadherins (Figure 4-1B). Using a parallel plate geometry, we applied step loads on the order of 10-50 nN to isolated colonies, and used force-feedback control to maintain a given load while recording colony deformation (Figure 4-S1B). Both MCF10A and MCF10AT colonies exhibited large initial displacements followed by continuous creep (Figure 4-2C). However, their responses were markedly different from each other. Pre-malignant MCF10AT colonies, given the same environmental conditions and time to grow, were significantly stiffer than phenotypically normal MCF10A colonies (two-sided t-test, $p=5.5x10^{-5}$).

The difference in compliance between MCF10A and pre-malignant MCF10AT colonies could primarily be due to three different factors (Figure 4-2D): (1) single cell mechanics, (2) cell-cell connection strength, or (3) changes in multicellular structure. To test single cells, we embedded MCF10A and MCF10AT cells in laminin-rich ECM as before, but extracted them after 12 hours for creep compression tests. MCF10AT single cells were not noticeably stiffer than MCF10A single cells (one-sided t-test, $p=0.329$), suggesting that the increased stiffness observed for pre-malignant colonies does not result from stiffer cells (Figure 4-3A). To test cell-cell connectivity, we extracted MCF10A and MCF10AT colonies after 6-8 days of growth. As suggested by previous literature [34], 6-8 day-old MCF10A

colonies did not yet have lumens (i.e. colonies were filled structures, Figure 4-S2). When healthy and pre-malignant colonies had the same multicellular structure, MCF10AT were once again not distinguishably stiffer than MCF10A colonies (Figure 4-3B, p=0.963). Changes in cell-cell connectivity would be present at the 6-8 day time point, suggesting that neither single cell mechanics nor cell connectivity accounted for the increased stiffness observed in "mature" pre-malignant colonies. Notably, both of the 6-8 day "filled" colonies (Figure 4-3B) exhibited similar creep response to "mature" MCF10AT colonies (Figure 4-2C). This suggested that lumen formation significantly decreased the stiffness of the colony.

Predicted mechanical property changes due to structural differences are consistent with measurements

As creep response of MCF10A and MCF10AT were only different upon lumen formation, we developed a computational model to investigate how differences in multicellular structure could affect the mechanical properties of the colonies. Constitutive modeling of cells has been previously considered by a number of authors. Some of the most detailed models made use of a biphasic approach, in which the cell cytosol was modeled as having both a solid phase and a fluid phase that interact [169, 170, 171, 172]. Similar approaches have also been extensively used to model collagen networks [169, 173]. However, because our measurements were on the multicellular scale and probed relatively small strains, we adopted a simpler modeling approach, whereby the acinus was modeled using the level set method [174] as an incompressible linear viscoelastic solid immersed in an incompressible fluid (see Simulation Development).

Within this simulation framework, there is a clear correspondence between the simulation parameters and the experimental measurements. Using a system identification method, we fit a standard linear solid (SLS) model to our single-cell experimental data and converted these results into simulation parameters (see Simulation Development). To investigate the effects of multicellular structure alone, we created hollow and filled models using identical material properties, with structure being the only difference between the two. Our model predicted approximately a 3-fold increase in compliance for a hollow structure (Figure 4-3C). This is on the same scale as the 1.6-fold increase observed in experiments (Figure 4-2C), suggesting that multicellular structure could be an important determinant of the mechanical properties of breast epithelial cell subunits.

Multicellular structure could affect perceived mechanical microenvironment independent of material properties

If multicellular structure affects the mechanical response of epithelial subunits, individual cells could mechanically sense these differences in structure. Epithelial cells have been shown to mechanosense through cadherin junctions [109], and disrupting these cadherin junctions causes formation of a disorganized, filled structure [89]. Here, we consider a simple case corresponding to when a cell undergoes a very small isotropic contraction, due to a small amount of fluid flow across the cell boundary. Considering the cell as a small control volume within the multicellular structure, we can apply small changes to this control volume as a simple model of cellular contraction. Using our multiphase simulation, we can model contraction and predict the force-displacement response of the surrounding structure. With this prediction, we can calculate a "perceived stiffness" for the cell based

only on the surrounding cells (see Simulation Development). We simulated single cells on the edges of both hollow and filled structures (Figure 4-4 A-B), and predict approximately a 15% increase in "perceived stiffness" due to lumen filling alone.

Discussion

We investigated changes to mechanical properties of a breast epithelial structure during lumen filling. Our data indicate that the filling of the lumen leads to about a 1.6-fold decrease in short-timescale creep compliance (i.e. increased stiffness). We observed this difference despite single MCF10A and MCF10AT cells having very similar mechanical properties, and multicellular structures pre-lumen formation not being detectably different from each other. From these data, we concluded that the arrangement of cells in the epithelial subunit could affect the mechanical properties of the structure itself.

Our results highlight a key role for tissue structure in the mechanosensing at the single cell level. Considering that a two-fold increase in matrix stiffness leads to lumen filling [57], a 15% increase in perceived stiffness due to multicellular structure alone could be a potentially significant step towards loss of structure and function in the mammary gland. In humans, many – but not all – filled-lumen structures progress to form malignant tumors [165]. As increased matrix stiffness drives the malignant phenotype through a contraction-mediated process [57], a 15% increase in perceived stiffness could further destabilize the equilibrium of a multicellular structure. Increased perceived stiffness could lead to a loss of contact inhibition [163] and eventually promote tumor progression [4] and invasion into the surrounding environment [66].

In order for this type of mechanical difference to be biologically significant, individual cells would have to be capable of mechanosensing through cadherins or other cell-cell junctions. A growing body of evidence suggests that cells can sense mechanical forces through cadherins. For example, vinculin localizes to E-cadherin when cells are pulled with cadherin-coated beads [109], similar to behavior observed with integrins [175]. Interestingly, cadherins also play an important role in morphogenesis and tumor growth. Blocking E-cadherin function in non-malignant breast epithelial cells leads to disorganized, non-polarized structures [89]. This has been previously shown to affect mechanical phenomena such as coherent rotation in breast epithelia [75]. The molecular mechanisms behind cadherin-based mechanosensing are still under investigation, and the techniques described here provide additional tools to study this process.

Simulation Development

Development of simulation framework

The simulations are carried out within a cube, using a right-handed coordinate system in which the z-axis points upwards (Figure 4-S3A). The cube is filled with a background fluid that is modeled using the Navier-Stokes equations

$$\rho\frac{\partial \mathbf{u}}{\partial t} + \rho(\mathbf{u}\cdot\nabla)\mathbf{u} = -\nabla p + \nu\nabla^2\mathbf{u}$$

with the incompressibility constraint

$$\nabla \cdot \mathbf{u} = 0 \qquad [1]$$

where ***u*** is the fluid velocity, ρ is the density of the fluid, p is the fluid pressure, and ν is the fluid viscosity. For the small length scales considered, the term $(\mathbf{u}\bullet\nabla)\mathbf{u}$ corresponding to the fluid inertia is negligible. This system of equations is simulated using the finite-difference method on a fixed rectangular grid, with the incompressibility constraint imposed via a finite-element projection step [176, 177].

The acinus is modeled using the level set method [174], which is well-suited for tracking deforming boundaries on a fixed rectangular grid. Within the acinus, the velocity follows the equation

$$\rho\frac{\partial \mathbf{u}}{\partial t} + \rho(\mathbf{u}\cdot\nabla)\mathbf{u} = -\nabla p + \nu\nabla^2\mathbf{u} + \nabla\cdot\sigma + \nabla\cdot\varsigma.$$

where σ is an elastic stress tensor, and ς is a viscoelastic stress tensor. Here, we assume that the density and viscosity of the acinus is the same as the fluid. Since we are interested in quasi-static behavior, the viscosity will not play a significant role, and since gravity in negligible at the small scales considered, the relative difference in density will have only a limited effect.

Since the material is incompressible, there is no notion of a bulk modulus due to volumetric deformations, and σ and ς are therefore traceless. For small strains, the two tensors can be updated using the equations

$$\frac{\mathcal{D}\sigma}{\mathcal{D}t} = 2\mu_0\mathbf{D}, \qquad \frac{\mathcal{D}\varsigma}{\mathcal{D}t} = 2\mu_1\mathbf{D} - 2\lambda\varsigma \qquad [2]$$

where the derivative D incorporates advection and tensor spin components, and $D = (\nabla u + (\nabla u)^T)/2$ is the rate-of-deformation tensor. Here μ_0 and μ_1 are the elastic and viscoelastic shear moduli respectively, and λ is a viscoelastic damping parameter. Equation 2 has a very similar form to the SLS model, and is a natural three-dimensional extension, with the parameters μ_0, μ_1, and λ being analogous to k_0, k_1, and η from a SLS 1-dimensional linear viscoelastic model.

To inform the simulation with properties based on our measurements, we used a system identification method to fit our creep data to the SLS model. This model (Figure 4-S4A) consists of a spring (k_1) in parallel with a spring-dashpot (k_0, η). As a check, the parameters obtained from this model (Figure 4-S4B-D) are qualitatively consistent with the data presented in Figures 4-2 and 4-3. While other models may also fit our data, we use the SLS model here simply to inform our simulation with a set of reasonable mechanical parameters.

To carry out the compression of an acinus, a horizontal plate is introduced into the simulation that is free to move in the vertical direction, onto which a constant downward force of F_p is applied. As it comes into contact with the acinus, it exerts a force on the acinus causing it to deform, until it reaches equilibrium. Figures 4-S3C and 4-S3D show typical snapshots of the simulation for a sphere to model the MCF10AT geometry, and a spherical

shell to model the MCF10A geometry. In Figure 4-S3D, four small tubes are placed in the acinus, since the acini in experiments are assumed not to be watertight, and allowing fluid to flow out of the lumen can affect the mechanical response. However, simulations using a watertight central cavity were also carried out.

Using the simulation to quantify the effects of geometry is simplified by the fact that the mechanical model is linear, and that the time scale for the acinus to reach quasistatic equilibrium, t_E, is much smaller than the viscoelastic relaxation time scale τ. Since the model is linear, if the elastic modulus is scaled by a factor α, then the force response for a given, fixed displacement will be scaled by α also. Over an intermediate time t_1, where $t_E \ll t_E \ll \tau$, the effective elastic modulus is given by $\mu_0 + \mu_1$, whereas over a much longer time t_2 where $\tau \ll t_2$, the effective elastic modulus is given by μ_0. The force response at t_2 will therefore be equal the force response at t_1 but scaled by a factor of $\mu_0/(\mu_0 + \mu_1)$. Because of this, it is possible to focus on simulations using elasticity only, setting $\mu_1 = \lambda = 0$. By carrying out severalsimulations with different displacements, a constant G representing a geometrical scaling factor can be obtained, so that $K_0 = G\mu_0$. By the above argument, it must also be true that $(K_0 + K_1) = G(\mu_0 + \mu_1)$ and thus $K_1 = G\mu_1$.

The simulations are carried out in dimensionless units that are differentiated from their physical counterparts by writing them with a tilde. To connect the simulations to experiments, a mass scale M, length scale L, and time scale T must be introduced, after which any simulation quantity can be related to a physical value by multiplying by the appropriate scales. The simulation cube has side length 3, the acinus has radius 1.1, and the fluid has unit density $\tilde{\rho} = 1$. In the MCF10A simulations, the shell has thickness 0.4, which was chosen based on the confocal microscope images in Figure 4-2. To model a 55μm diameter acinus, a length scale of L=25 is chosen, and by assuming the density is close to that of pure water, so that $\rho = 10^3$, then the mass scale must be

$$M = 10^3 \times L^3 = 1.56 \times 10^{-11}.$$

For each acinus geometry, simulations over a range of plate forces were carried out, using $\tilde{\mu} = 1$ and $\mu_1 = \lambda = 0$. For each simulation, the change in height of the acinus once it has reached equilibrium is recorded. By carrying out a linear fit of the height changes with respect to the plate force, a spring constant $\widetilde{K}_0$ can be calculated. To estimate the shear modulus of the acinus, the value of $\widetilde{K}_0 = 0.0193$ for the solid sphere is compared to the value $K_0 = 0.018$ from experiment. Since

$$\widetilde{K}_0 = \frac{K_0 T^2}{M}$$

it follows that the time scale is

$$T = \sqrt{\frac{M\widetilde{K}_0}{K_0}} = 3.35 \times 10^{-5}.$$

Hence the shear modulus is

$$\mu = \frac{\tilde{\mu} M}{LT^2} = 557.$$

For an incompressible material where the Poisson ratio is 0.5, the Young's modulus is $E = 3\mu = 1670$. With the physical scales now calibrated, the simulation data of plate force against height change can now be plotted in physical units as in Figure 4-3C. This figure

gives a value of K_0 for the MCF10A acinus as 0.0055. The three-fold difference is roughly similar to the differences in the 1.6-fold difference in experimental measures for K_0, and thus it is consistent that the differences could be explained by geometry.
Figures 4-S3A and 4-S3B show plots of pressure in a vertical cross-section through the hollow and filled acini. As would be expected, regions of higher pressure are visible at the locations where the plate and bottom surface make contact. However, in the hollow simulation, a region of negative pressure is also visible, as the interior part of the shell is stretched during the deformation.

Simulations of perceived stiffness

Suppose first that a single cell is centered at the origin in three-dimensional material that is incompressible with Young's modulus, *E*, which initially has no stress within it. A spherical region *S* centered on the origin with radius *R* can be introduced, where *R* is chosen to be large enough to enclose the cell. Suppose that the cell's volume decreases by a very small amount *V*. If the radial symmetry is assumed, then it can be analytically derived (Supplemental Information) that the components of the stress tensor $\boldsymbol{\sigma}$ can be expressed in spherical coordinates (r, θ, ϕ) as

$$\sigma_{rr} = \frac{EV}{3\pi r^3}, \qquad \sigma_{\theta\theta} = \sigma_{\phi\phi} = -\frac{EV}{6\pi r^3},$$
$$\sigma_{r\theta} = \sigma_{r\phi} = \sigma_{\theta\phi} = 0. \qquad \textbf{[3]}$$

The total force exerted on the spherical region can therefore be calculated by integrating the radial coordinate of the stress tensor over the surface of sphere ϕS to obtain

$$F = \int_{\phi S} \mathbf{n} \cdot \boldsymbol{\sigma} \cdot \mathbf{n}\, dS = 4\pi R^2 \frac{EV}{3\pi R^3} = \frac{4EV}{3R}.$$

It therefore follows that force exerted on the cell will be proportional to the shear modulus of the material. This provides a method in which cells can probe their local environment: if a cell contracts by a volume V and experiences a total radial force F, then the perceived shear modulus of the nearby material is given by

$$E = \frac{3RF}{4V}. \qquad \textbf{[4]}$$

Using the simulations, we can now address how the effective shear modulus will vary depending on where a cell is situated within a given geometry. To carry this out, we modify the incompressibility condition of Equation 1 to include a small volume removal, with the form

$$\tilde{\nabla} \cdot \tilde{\mathbf{u}} = \tilde{c}(1 - \cos 2\pi\tilde{t})(\tilde{q} - |\tilde{\mathbf{x}} - \tilde{\mathbf{x}}_c|)$$

for $\tilde{t} < 1$ and $|\tilde{X} - X_c| < \tilde{q}$. Values of the simulation constants of $\tilde{q} = 0.5$, $\tilde{c} = 0.15$, and $R = \widetilde{0.25}$ were used, corresponding to a removal of 307μm² in physical units.

Three simulations carried out for a contraction in the center of a sphere, at the edge of a sphere, and at the edge of a spherical shell. For each one, the effective stiffness that a cell

would perceive, using Equation 4, is shown in Figure 4-4C. In the center of the sphere, the effective stiffness closely matches the real stiffness of the material, as would be expected for a cell in an infinite medium. However, the stiffness is significantly lessened for the other two simulations, particularly for the spherical shell. While the precise reductions in perceived stiffness are dependent on the parameters used, a marked drop in perceived stiffness and a difference depending on the geometrical configuration of the cells appear to be general features. Using the parameters described here yields a 15% drop in stiffness due to lumen formation alone.

Figures 4-4A and 4-4B show plots of the magnitude of the deviatoric stress tensor, computed as $|\sigma - 1(\mathrm{tr}\ \sigma)|$, for a contraction at the edge of sphere and spherical shell respectively. This quantity provides a useful scalar measure of shear stress, and for this case is more instructive than examining pressure, given that the analytic solution in Equation 3 predicts zero pressure. As expected, the shear stresses decay rapidly as a function of distance from the contraction region. Shear stresses are slightly higher for the spherical shell, since it provides less resistance to deformation.

Methods

Cell culture

Mammary epithelial cells (MCF10A, Ha-Ras MCF10AT) were stably transfected with a lentiviral tet-off promoter to express Histone-H2B labeled with eGFP ([178], Addgene plasmid 21210). Following a previously established protocol [34], cells were cultured in DMEM/F12 (UCSF Cell Culture Facility) supplemented with 5% horse serum (Invitrogen), 20 ng/mL EGF (Peprotech), 0.5 μg/mL hydrocortisone (Sigma), 100 ng/mL cholera toxin (Sigma), 10 μg/mL insulin (Sigma) and 1x penicillin/streptomycin (Invitrogen). Cells were passaged using 0.05% trypsin-EDTA (UCSF).

Cells were then fully embedded in laminin-rich, growth-factor reduced extracellular matrix (Matrigel™, BD Biosciences) at a concentration of approximately 100 cells/mL using previously described methods [34, 37]. Cells embedded in gels were fed with DMEM/F12 supplemented with 2% horse serum, 5 ng/mL EGF, 0.5 μg/mL hydrocortisone, 100 ng/mL cholera toxin, 10 μg/mL insulin and 1x penicillin/streptomycin. For single cell experiments, cells were extracted from the lrECM gels after 12 hours. For multicellular experiments, structures were extracted either between days 6-8 or days 15-21. Measurements were not noticeably different as a function of number of days in culture.

Immunofluorescence

Embedded structures fixed as previously described [37]. Structures were pipetted directly onto a glass slide and fixed with 4% paraformaldehyde in phosphate-buffered saline (PBS). Samples were washed with PBS, permeabilized with 1% Triton-X 100, and blocked with 3% BSA in PBS. Samples were stained with anti-α_6-integrin (BD Pharmingen 562473, 1:500) and mounted with ProLong Gold antifade reagent (Invitrogen). Images were taken on a Yokogawa spinning disk confocal microscope on a Zeiss Axio Observer Z1 using a thermoelectrically cooled Cascade II EMCCD and a 20x 0.4NA objective.

Extraction from 3D culture

Single cells and colonies were extracted from the lrECM gels for AFM study with an adapted version of previously described colony-extraction method [37]. The lrECM gels were quickly washed with PBS and then mechanically detached from the culture well. To dissolve the matrix, embedded gels were soaked in a cold PBS-EDTA mixture (0.5 M EDTA pH8.0 from Invitrogen diluted to 5.5μM final concentration in PBS) for 10 minutes before being placed in a 1.5~mL tube with excess PBS-EDTA for an additional 25 minutes. The resulting mixture was gently centrifuged at 100-200g (single cells 3-5 minutes/colonies ~10s) and the supernatant was aspirated away. Cells/colonies were resuspended in CO2-independent media (Invitrogen) with 10% fetal bovine serum and 1x penicillin-streptomycin and plated on a poly-L-lysine-coated (MW>300,000, P5899 Sigma-Aldrich) cover slip for AFM experiments. Poly-L-lysine coatings were used to allow samples to electrostatically attach without activating cell adhesion machinery on the surface.

Surface preparation

Custom chambers for AFM experiments were made by UV-gluing custom laser-cut acrylic walls (3mm tall) to a pre-cleaned (KOH base bath) cover slip. Chambers were coated with poly-L-lysine immediately before the experiments by incubating for 20 minutes with a 0.1 mg/mL solution of poly-L-lysine in PBS. Chambers were washed ten times with deionized water and dried with a nitrogen stream before plating samples.

Atomic force microscopy

AFM experiments were performed on a modified Veeco Bioscope I mounted on a Zeiss Axiovert 25 inverted microscope [100] and a Veeco Catalyst mounted on a Zeiss Axio Observer Z1. Tipless silicon nitride MLCT (30-50 nN/μm, Veeco) cantilevers were used for multicellular experiments, and tipless Arrow cantilevers (10-20 nN/μm, Nanoworld) were used for single cell experiments. Force steps were applied to the samples using a closed-loop piezoelectric, and sample deformation were measured over time. Data analysis was performed on the force reduction step, after a series initial compression and relaxation steps that ensured good contact between the samples and both the cantilever and substrate. Experiments were performed at 37C and completed within 2 hours of plating on poly-L-lysine. There was no discernible change in measured mechanical properties over the course of the experiment. Each sample was also imaged in brightfield and eGFP epifluorescence (nuclei), and its position on the coverslip was recorded to prevent duplicate testing of the same sample.

Parameter fitting

Quantification of the compliance of acini and single cells was performed using techniques from system identification. A three-parameter SLS model, as shown in Figure 4-S4A, is a simple linear viscoelastic system that can capture the observed instantaneous response followed by an exponential decay. We selected an eight-second interval, beginning with the force step, to fit the data to a Kelvin body parameterized by k0, k1, and η.

The parameter fitting was accomplished by first downsampling with a moving average at 5~Hz to filter out high-frequency noise. Next, Matlab's `idgrey' was used to solve for the

state-space parameters of the first-order ODE for a SLS body, given an initial guess. To ensure a valid solution, the output SLS body was then simulated with the measured force input. The simulated SLS body and actual measured displacements were compared visually to ensure a reasonable fit to the data. SLS fits that were very far from the measured response were discarded, usually due to noise in the measurement.

Statistical tests

Creep compliances were compared at 8s time points using t-tests as described in the results section with $p<0.05$ as the significance threshold.

Acknowledgements

We would like to thank Matt Paszek and Luke Cassereau for providing GFP-H2B labeled cells. Thanks to the members of the Sethian, Weaver, Fletcher and Bissell Labs for helpful comments and feedback on the manuscript.

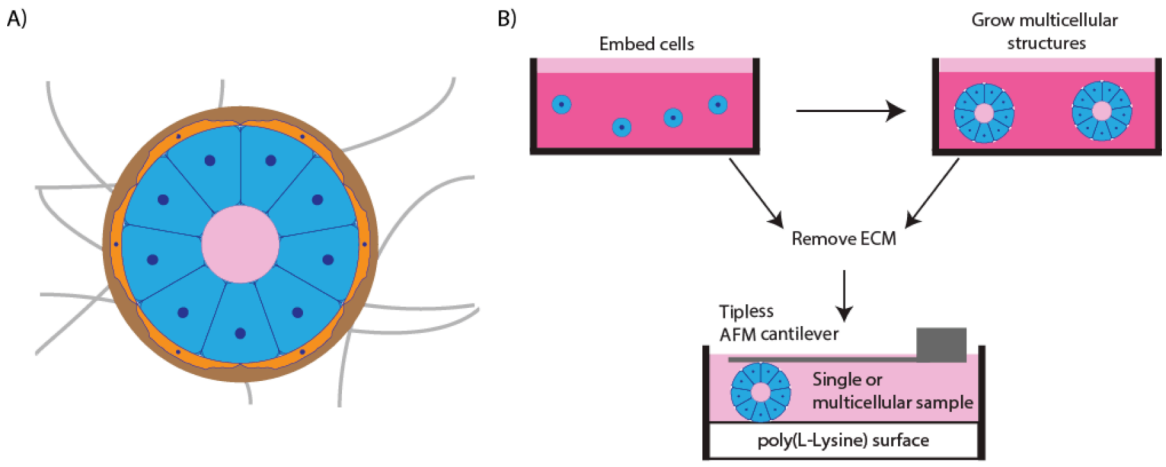

Figure 4-1: (A) A mammary epithelial cell grows in a dynamic environment surrounded by extracellular matrix, fluids, and other cells. (B) Mammary epithelial cells grown in laminin-rich extracellular matrix can be extracted and mechanically probed at single and multicellular states using identical trypsin-free extraction methods.

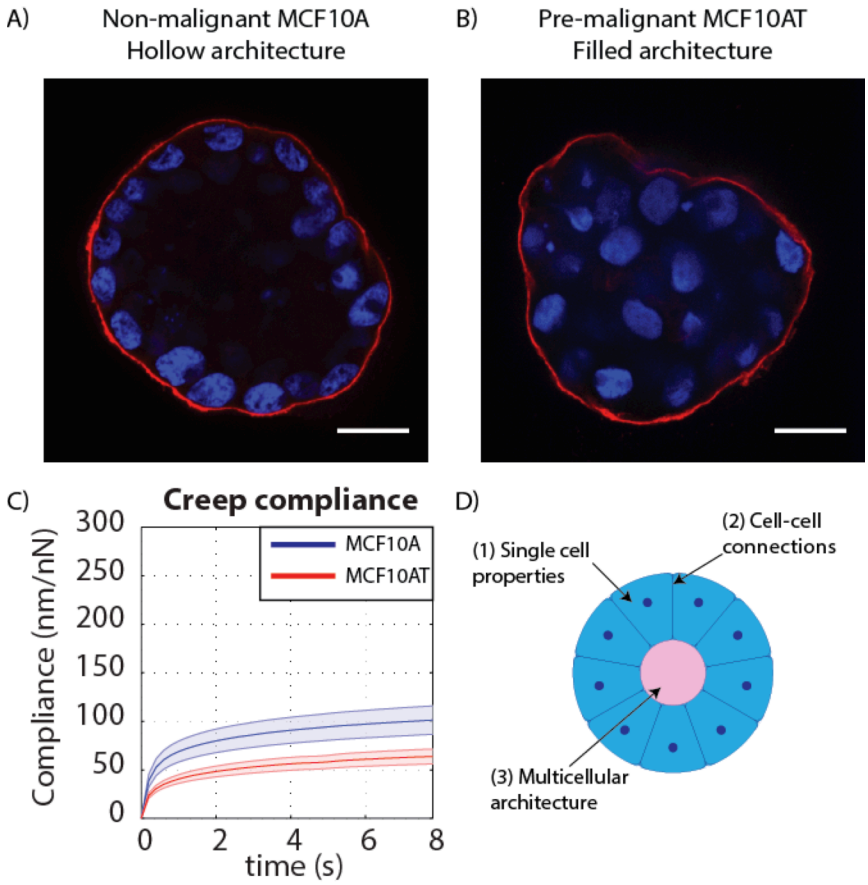

Figure 4-2: Confocal immunofluorescence images of (A) non-malignant MCF10A (hollow lumen) and (B) pre-malignant MCF10AT (filled lumen) colonies. Scale bars 25µm. (C) Creep compliance (mean +/- 95% CI) of hollow and filled breast epithelial colonies. (N=32 and 31 colonies for A and T) (D) Differences in mechanical response could be due to (1) different properties of single cells (2) changes in connectivity or (3) changes in multicellular architecture.

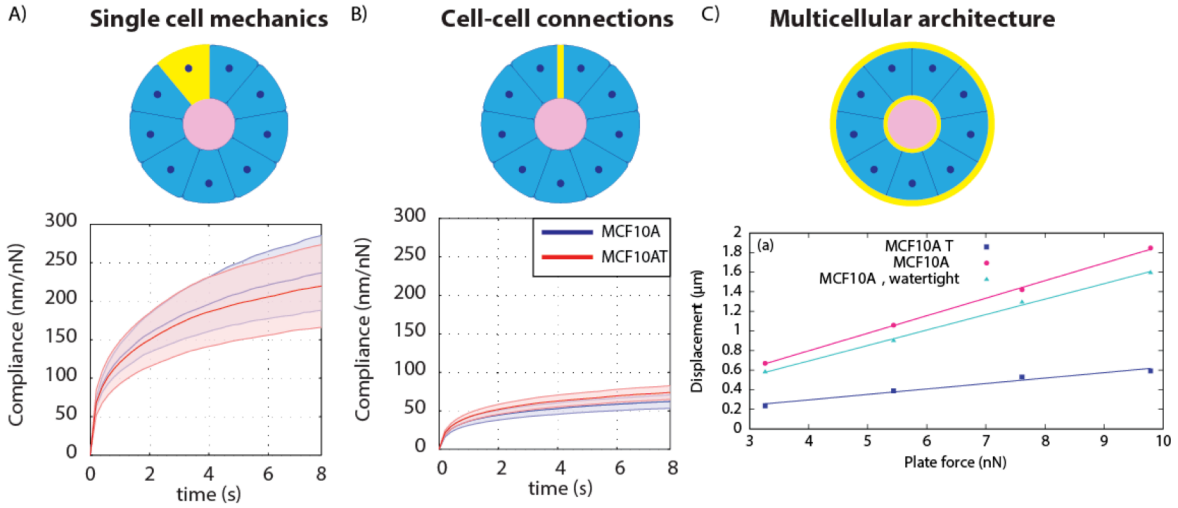

Figure 4-3: Creep compliance (mean +/- 95% CI) of MCF10A and MCF10AT cells at (A) single cell state (N=14 and 15 cells for A and T) and (B) 6-8 day state before lumen formation (N=34 and 33 colonies for A and T). (C) Simulation of hollow and filled structures predicts decreased compliance (increased stiffness) of the structure associated with multicellular architecture.

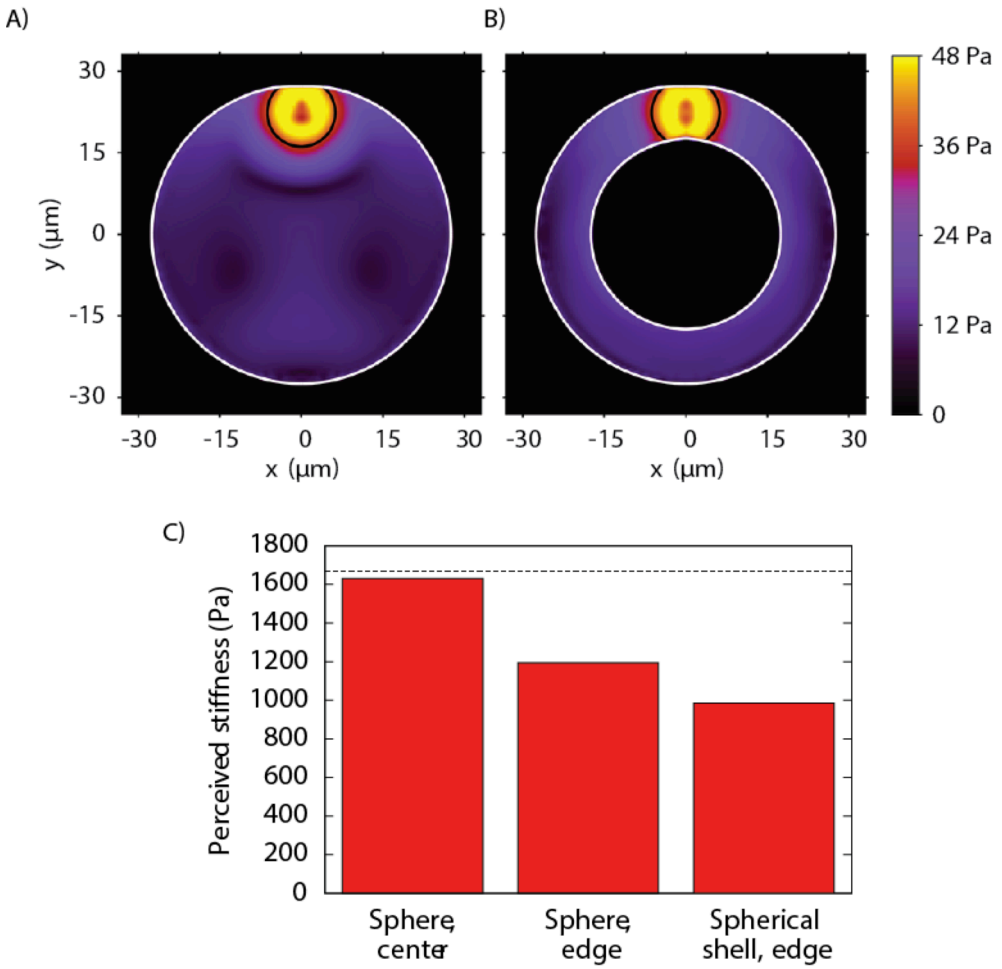

Figure 4-4: Cross-section through 3D simulations of single cell contraction in (A) filled and (B) hollow structures. (C) Perceived stiffness for a single cell in a hollow structure is approximately 15% lower than a filled structure.

Supporting Information

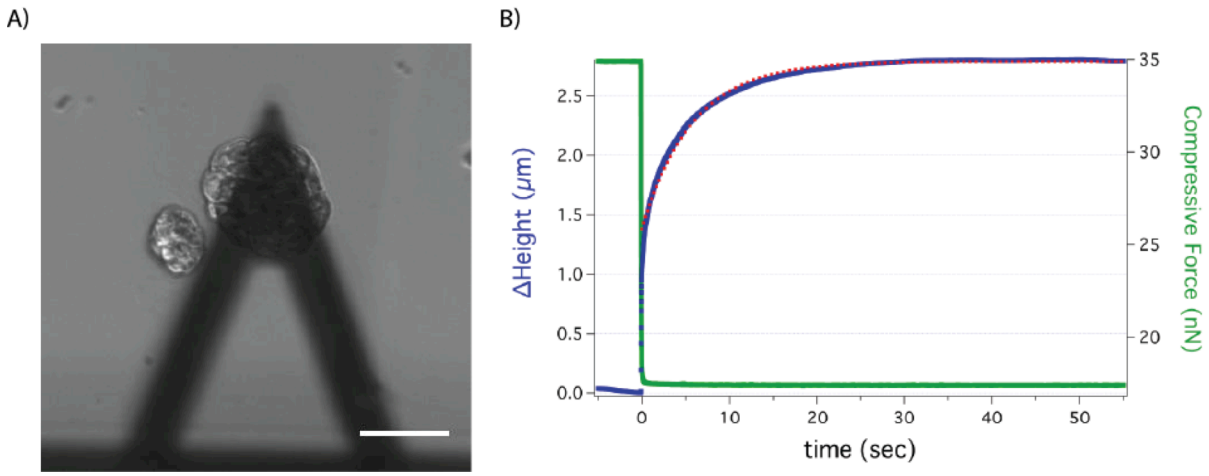

Figure 4-S2: (A) Example image of an MCF10A acinus under a tipless atomic force microscope cantilever. Scale bar 50μm. (B) Representative creep response of an MCF10A acinus.

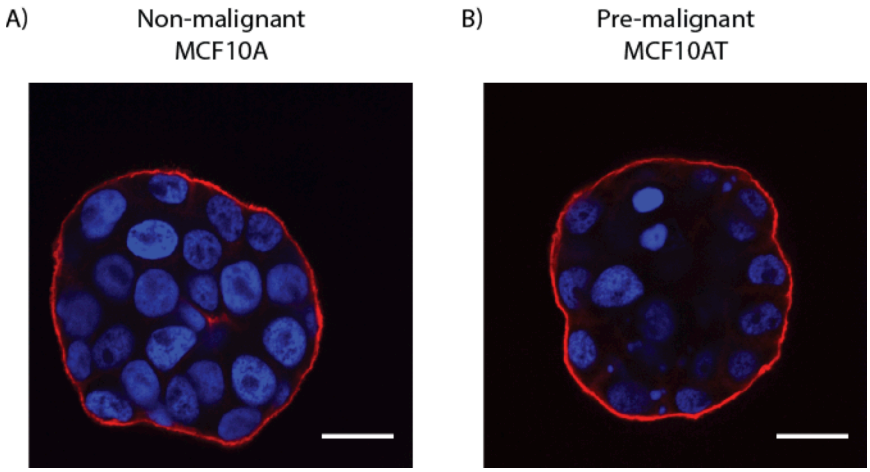

Figure 4-S1: (A) Confocal immunofluorescence images of 8 day colonies of (A) MCF10A and (B) MCF10AT. 6-8 day time points were selected for testing because this was before lumens formed. Scale bars 25μm.

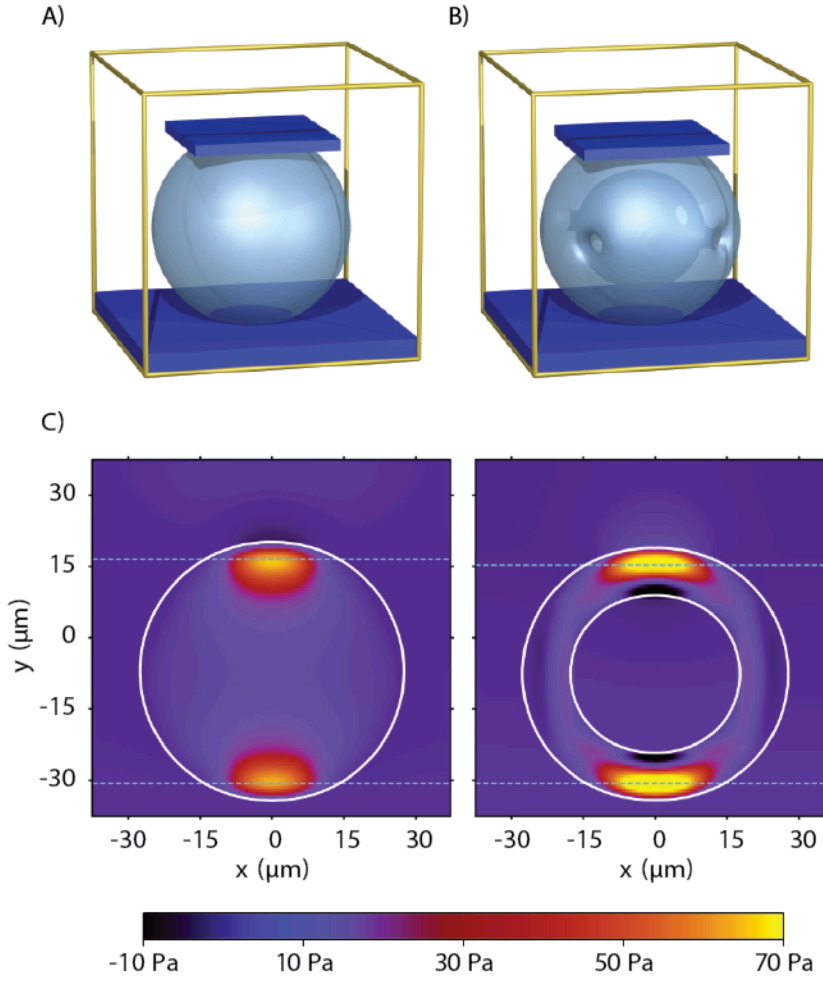

Figure 4-S3: (A-B) Visualization of the 3D plate compression simulation environment used in this study. (C) Cross-section through 3D simulation of plate for hollow and filled structures.

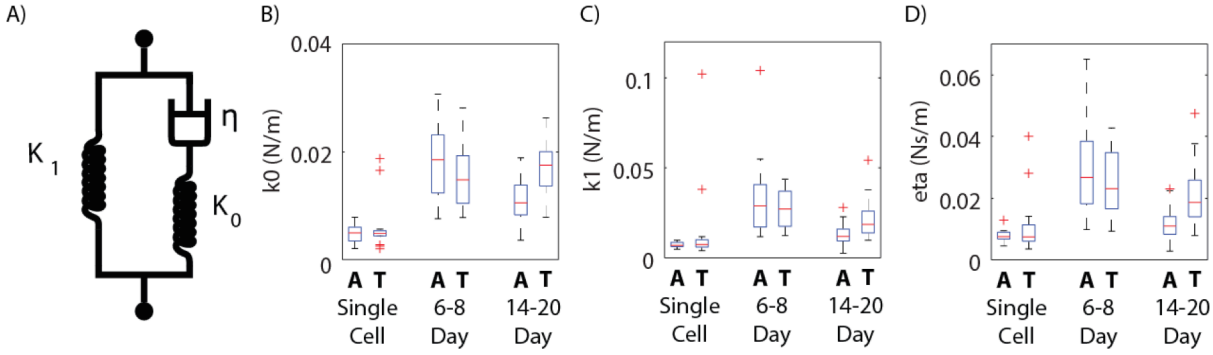

Figure 4-S4: (A) Standard Linear Solid model and (B-D) relevant parameters measured by fitting creep curves using system identification techniques. Fit parameters were used to extract mechanical properties for the model.

Chapter 5: Conclusion

Matrix stiffness has been widely implicated in morphogenesis and malignancy. The work presented here suggests that external forces can play an equally important role. External forces directed migration by aligning collagen fibers (Chapter 2), and also encouraged malignant cells to re-enter acinar morphogenesis (Chapter 3). The multicellular structure itself also mattered, as lumen filling during malignant progression increases stiffness of isolated cellular structures enough to potentially destabilize mechanical equilibrium (Chapter 4). With the data presented here, technical advances – particularly in three-dimensional matrix biology and genomics – have the potential to identify a host of novel molecular mechanisms involved in mechanosensing, migration, polarity establishment, and cell-cell communication.

Summary of findings

In Chapter 2, we presented a new deformable silicone chamber designed to apply step compression to cell-embedded ECM gels. This device is relatively inexpensive, amenable to long-term culture, and compatible with basic microscopy and immunostaining techniques. We used this silicone chamber to compress mouse mammary epithelial cell aggregates embedded in a Type I collagen matrix. Compression aligned collagen fibers perpendicular to the axis of compression and directed branch growth along these aligned fibers. Unlike most mechanosensing (i.e. stiffness sensing) phenomena, inhibiting RhoA-mediated contractility did not prevent branching or alignment sensing. Alignment sensing was dependent on fascin instead. This finding is consistent with canonical motility functions of RhoA and fascin. RhoA is associated with contractions [179]; contractions that were needed here to align collagen networks, but not to follow them. Fascin is associated with filopodia formation [180], a probing mechanism which plausibly could be used by the cell to sense alignment.

We then studied the effects of compression on tumorigenesis of human breast epithelial cells embedded in laminin-rich ECM in Chapter 3. We found that transient applied stress 'phenotypically reverted' cells to a less malignant phenotype reminiscent of acinar morphogenesis. Surprisingly, compression did not alter proliferation rate. Using time-lapse microscopy, we found that compression encouraged cells to re-enter the 'correct' morphogenetic program and form spherical, hollow acini. However, compression-induced growth inhibition did not work if E-cadherin function was blocked, suggesting the importance of cell-cell communication in translating this signal.

Having discovered that external forces could affect multicellular structure, we investigated how changes in structure could affect mechanosensing in a multicellular tissue subunit in Chapter 4. We used an AFM to measure mechanical property changes associated with lumen filling as a model of human breast epithelial carcinoma. We observed that filled-lumen structures were approximately 1.6 times stiffer, and that this phenomenon could not be attributed to single cell mechanics or cell-cell connection strength. Using a multiphase computational model, we predicted that lumen geometry alone could account for increased

stiffness on the scale observed in our measurement. Based on our finding in Chapter 3 that cell-cell communication was important for mechanosensing, we used our model to simulate the mechanical microenvironment of a single cell within the multicellular subunit. A single cell's 'perceived stiffness' could increase due to lumen filling and potentially contribute to malignant progression.

Future directions

At any moment in time, there are countless simultaneous morphological processes occurring in the body. Despite so many things that could go wrong, the human body works so often. As Mina Bissell always says, "There are 10-70 trillion cells in your body. If even 0.0001% of them got cancer, you'd be a giant lump of cancer." We have only just begun to understand how a single cell becomes a human form. As biochemical and engineering technology progresses, cell mechanics studies on gene expression timescales are becoming progressively more accessible. Within morphogenesis and tumor mechanics, there are many immediate and long-term follow-up opportunities based on the continuously growing body of literature.

One of the most exciting possibilities in our reversion assay is the possibility that compression could induce milk production. Placing cells in the correct biochemical and biophysical environment is important for milk production [42]. Just as compression encourages malignant cells to undertake a less malignant phenotype, it may encourage non-malignant cells to become even healthier. We performed some initial experiments studying compression-induced β-casein expression in compressed non-malignant HMT3522-S1 cells, but chose to focus on reversion instead.

All of the ECM gels used in this work viscoelastically relax to zero stress on timescales much faster than morphogenesis and tumorigenesis (minutes vs. days). It remains quite surprising that a transient stress could provide such a dramatic responses, particularly in the non-stress stiffening regime of laminin-rich ECM. It is plausible that polarity changes at very early time points contribute to compression-induced phenotypic reversion. Further investigation into the mechanics of polarity formation in our system could help us better understand this process.

The time-dependence of compression is another variable of interest. Time lapse studies have shown that healthy cells exhibit coherent rotation and synchronized division during acinar morphogenesis [75]. Once cells have begun growing in a malignant fashion, it would be interesting to find out if they eventually become insensitive to compression. As pre-aggregated clusters of healthy cells neither coherently rotate nor form acini [75], it is possible that malignant clusters beyond a certain size become insensitive to mechanics. Understanding important time points would provide some clue of which cellular processes to further investigate.

A time frame may be particularly useful with the advent of whole-genome shotgun sequencing [181]. It is becoming progressively cheaper to sequence the entire transcriptome in an unbiased fashion using deep-sequencing technologies [182]. We are

currently working to use this technology to measure expression differences in malignant cells in response to compression. Our hope is to identify early (~1 day) and late (~8-10 day) genetic differences to better understand the complex network morphogenetic changes. This technique will fundamentally change the way biology researchers approach mechanistic changes on transcriptional timescales.

Single cell techniques combined with whole genome processing will be quite powerful. Once potential targets are identified, single cell multiplex sequencing can already be used to detect rare mutations [183], and live cell molecular beacon techniques report the localization of mRNA in real time [184]. Molecular beacons could be very useful in understanding mechanosensing differences in 3D structures, as we don't expect these structures to be homogeneous.

There is also work to be done on the side of the microenvironment. Currently, we study morphogenesis and tumorigenesis in collagen and basement membrane ECM gels. However, the real breast has many more components like adipocytes, fibroblasts, macrophages, and blood vessels. Adipocytes, long thought to be simple energy stores, actually play a significant endocrine role, secreting estrogen [185] and interleukin-6 [186]. Early experiments with adipocyte/breast carcinoma co-culture suggest that adipocytes could promote carcinoma growth [187, 188]. Adding more complex players to the culture system and studying the resultant mechanical interactions has the potential to make mechanotransduction research much more readily translatable *in vivo*.

Another variable we considered but did not end up focusing on in this work is time-dependent loading. Studies in cartilage indicated that static loads are processed very differently than cyclic loads. Cyclic loads encouraged matrix protein synthesis [189], while static loads decreased protein synthesis and increased interleukin expression (IL-1) [153, 189]. Interleukins (IL-25) have recently been discovered to be an autocrine tumor suppressor secreted by healthy breast epithelial cells [190]. As interleukins can be mechanically expressed and are potential tumor suppressors, a more detailed study of interleukin expression in epithelial cells could provide insights into tumor suppression. (Protip: If you want to go into cancer research, read a bit about musculoskeletal research, and vice versa.)

There are plenty of interesting ideas out there. These are just a few of the ones that I wish I'd had more time to pursue. The more we learn about the human body, the more we find that everything is interconnected. Perhaps this is not so surprising, as interaction is the essence of being. I'm glad that I've been able to contribute a fraction of a small piece to our collective self-understanding. My time here was truly the breast.

References

1. DeSantis, C., Siegel, R., Bandi, P., & Jemal, A. Breast cancer statistics, 2011. *CA: A Cancer Journal for Clinicians*. (2011)
2. Howard, B. A. & Gusterson, B. A. Human Breast Development. *Journal of Mammary Gland Biology and Neoplasia*. (2000)
3. Medina, D. The mammary gland: a unique organ for the study of development and tumorigenesis. *Journal of Mammary Gland Biology and Neoplasia*. (1996)
4. Levental, K. R., Yu, H., Kass, L., Lakins, J. N., Egeblad, M., Erler, J. T., Fong, S. F. T., Csiszar, K., Giaccia, A., & Weninger, W. Matrix crosslinking forces tumor progression by enhancing integrin signaling. *Cell*. (2009)
5. Rahimi, N., Saulnier, R., Nakamura, T., Park, M., & Elliott, B. Role of hepatocyte growth factor in breast cancer: a novel mitogenic factor secreted by adipocytes. *DNA and Cell Biology*. (1994)
6. Orimo, A., Gupta, P. B., Sgroi, D. C., Arenzana-Seisdedos, F., Delaunay, T., Naeem, R., Carey, V. J., Richardson, A. L., & Weinberg, R. A. Stromal fibroblasts present in invasive human breast carcinomas promote tumor growth and angiogenesis through elevated SDF-1/CXCL12 secretion. *Cell*. (2005)
7. Gouon-Evans, V., Rothenberg, M. E., & Pollard, J. W. Postnatal mammary gland development requires macrophages and eosinophils. *Development*. (2000)
8. Affolter, M., Bellusci, S., Itoh, N., Shilo, B., Thiery, J. P., & Werb, Z. Tube or not tube: remodeling epithelial tissues by branching morphogenesis. *Developmental Cell*. (2003)
9. Ewald, A. J., Brenot, A., Duong, M., Chan, B. S., & Werb, Z. Collective Epithelial Migration and Cell Rearrangements Drive Mammary Branching Morphogenesis. *Developmental Cell*. (2008)
10. Fata, J., Werb, Z., & Bissell, M. Regulation of mammary gland branching morphogenesis by the extracellular matrix and its remodeling enzymes. *Breast Cancer Res*. (2004)
11. Hayakawa, T., Kishi, J., & Nakanishi, Y. Salivary gland morphogenesis: possible involvement of collagenase. *Matrix Suppl*. (1992)
12. Moore, K. A., Huang, S., Kong, Y. P., Sunday, M. E., & Ingber, D. E. Control of embryonic lung branching morphogenesis by the Rho activator, cytotoxic necrotizing factor 1. *Journal of Surgical Research*. (2002)
13. Wessells, N. K. & Cohen, J. H. Effects of collagenase on developing epithelia in vitro: Lung, ureteric bud, and pancreas. *Developmental Biology*. (1968)
14. O Brien, L. E., Zegers, M. M. P., & Mostov, K. E. Building epithelial architecture: insights from three-dimensional culture models. *Nature Reviews Molecular Cell Biology*. (2002)
15. Simian, M., Hirai, Y., Navre, M., Werb, Z., Lochter, A., & Bissell, M. J. The interplay of matrix metalloproteinases, morphogens and growth factors is necessary for branching of mammary epithelial cells. *Development*. (2001)
16. Nelson, C. M., Vanduijn, M. M., Inman, J. L., Fletcher, D. A., & Bissell, M. J. Tissue geometry determines sites of mammary branching morphogenesis in organotypic cultures. *Science*. (2006)
17. Hennighausen, L. & Robinson, G. W. Signaling pathways in mammary gland development. *Developmental Cell*. (2001)

18. Alford, D., Baeckstrom, D., Geyp, M., Pitha, P., & Taylor-Papadimitriou, J. Integrin-matrix interactions affect the form of the structures developing from human mammary epithelial cells in collagen or fibrin gels. *Journal of Cell Science*. (1998)
19. Klinowska, T., Soriano, J. V., Edwards, G. M., Oliver, J. M., Valentijn, A. J., Montesano, R., & Streuli, C. H. Laminin and beta1 integrins are crucial for normal mammary gland development in the mouse. *Developmental Biology*. (1999)
20. Wiseman, B. S., Sternlicht, M. D., Lund, L. R., Alexander, C. M., Mott, J., Bissell, M. J., Soloway, P., Itohara, S., & Werb, Z. Site-specific inductive and inhibitory activities of MMP-2 and MMP-3 orchestrate mammary gland branching morphogenesis. *The Journal of Cell Biology*. (2003)
21. Friedl, P. & Gilmour, D. Collective cell migration in morphogenesis, regeneration and cancer. *Nature Reviews Molecular Cell Biology*. (2009)
22. Wolf, K., Wu, Y. I., Liu, Y., Geiger, J., Tam, E., Overall, C., Stack, M. S., & Friedl, P. Multi-step pericellular proteolysis controls the transition from individual to collective cancer cell invasion. *Nature Cell Biology*. (2007)
23. Aman, A. & Piotrowski, T. Wnt/β-catenin and Fgf signaling control collective cell migration by restricting chemokine receptor expression. *Developmental cell*. (2008)
24. Gaggioli, C., Hooper, S., Hidalgo-Carcedo, C., Grosse, R., Marshall, J. F., Harrington, K., & Sahai, E. Fibroblast-led collective invasion of carcinoma cells with differing roles for RhoGTPases in leading and following cells. *Nature Cell Biology*. (2007)
25. Kouros-Mehr, H. & Werb, Z. Candidate regulators of mammary branching morphogenesis identified by genome-wide transcript analysis. *Developmental Dynamics*. (2006)
26. Martin, A. C., Kaschube, M., & Wieschaus, E. F. Pulsed contractions of an actin--myosin network drive apical constriction. *Nature*. (2008)
27. Grille, S. J., Bellacosa, A., Upson, J., Klein-Szanto, A. J., Van Roy, F., Lee-Kwon, W., Donowitz, M., Tsichlis, P. N., & Larue, L. The protein kinase Akt induces epithelial mesenchymal transition and promotes enhanced motility and invasiveness of squamous cell carcinoma lines. *Cancer Research*. (2003)
28. Kalluri, R. & Neilson, E. G. Epithelial-mesenchymal transition and its implications for fibrosis. *Journal of Clinical Investigation*. (2003)
29. Bailey, J. M., Singh, P. K., & Hollingsworth, M. A. Cancer metastasis facilitated by developmental pathways: Sonic hedgehog, Notch, and bone morphogenic proteins. *Journal of Cellular Biochemistry*. (2007)
30. Bello-DeOcampo, D., Kleinman, H. K., Deocampo, N. D., & Webber, M. M. Laminin-1 and α6β1 integrin regulate acinar morphogenesis of normal and malignant human prostate epithelial cells. *The Prostate*. (2001)
31. Golosow, N. & Grobstein, C. Epitheliomesenchymal interaction in pancreatic morphogenesis. *Developmental Biology*. (1962)
32. Wessells, N. K. & Cohen, J. H. Early pancreas organogenesis: morphogenesis, tissue interactions, and mass effects. *Developmental Biology*. (1967)
33. Davis, M. A. & Reynolds, A. B. Blocked acinar development, E-cadherin reduction, and intraepithelial neoplasia upon ablation of p120-catenin in the mouse salivary gland. *Developmental Cell*. (2006)
34. Debnath, J., Muthuswamy, S. K., & Brugge, J. S. Morphogenesis and oncogenesis of MCF-10A mammary epithelial acini grown in three-dimensional basement membrane cultures.

Methods. (2003)
35. Lelièvre, S. A., Weaver, V. M., Nickerson, J. A., Larabell, C. A., Bhaumik, A., Petersen, O. W., & Bissell, M. J. Tissue phenotype depends on reciprocal interactions between the extracellular matrix and the structural organization of the nucleus. *Proceedings of the National Academy of Sciences*. (1998)
36. Weaver, V. M., Petersen, O. W., Wang, F., Larabell, C. A., Briand, P., Damsky, C., & Bissell, M. J. Reversion of the malignant phenotype of human breast cells in three-dimensional culture and in vivo by integrin blocking antibodies.. *Journal of Cell Biology*. (1997)
37. Lee, G. Y., Kenny, P. A., Lee, E. H., & Bissell, M. J. Three-dimensional culture models of normal and malignant breast epithelial cells. *Nature Methods*. (2007)
38. Streuli, C. H., Bailey, N., & Bissell, M. J. Control of mammary epithelial differentiation: basement membrane induces tissue-specific gene expression in the absence of cell-cell interaction and morphological polarity. *Journal of Cell Biology*. (1991)
39. Muschler, J., Lochter, A., Roskelley, C. D., Yurchenco, P., & Bissell, M. J. Division of labor among the alpha6beta4 integrin, beta1 integrins, and an E3 laminin receptor to signal morphogenesis and beta-casein expression in mammary epithelial cells.. *Mol Biol Cell*. (1999)
40. Bello-DeOcampo, D., Kleinman, H. K., & Webber, M. M. The role of alpha 6 beta 1 integrin and EGF in normal and malignant acinar morphogenesis of human prostatic epithelial cells. *Mutation Research*. (2001)
41. Howlett, A. R., Bailey, N., Damsky, C., Petersen, O. W., & Bissell, M. J. Cellular growth and survival are mediated by beta 1 integrins in normal human breast epithelium but not in breast carcinoma. *Journal of Cell Science*. (1995)
42. Alcaraz, J., Xu, R., Mori, H., Nelson, C. M., Mroue, R., Spencer, V. A., Brownfield, D., Radisky, D. C., Bustamante, C., & Bissell, M. J. Laminin and biomimetic extracellular elasticity enhance functional differentiation in mammary epithelia. *EMBO J*. (2008)
43. Wewer, U. M., Shaw, L. M., Albrechtsen, R., & Mercurio, A. M. The integrin alpha 6 beta 1 promotes the survival of metastatic human breast carcinoma cells in mice. *The American Journal of Pathology*. (1997)
44. Yao, E. S., Zhang, H., Chen, Y. Y., Lee, B., Chew, K., Moore, D., & Park, C. Increased β1 integrin is associated with decreased survival in invasive breast cancer. *Cancer Research*. (2007)
45. Friedrichs, K., Ruiz, P., Franke, F., Gille, I., Terpe, H. J., & Imhof, B. A. High expression level of α6 integrin in human breast carcinoma is correlated with reduced survival. *Cancer Research*. (1995)
46. Wang, F., Weaver, V. M., Petersen, O. W., Larabell, C. A., Dedhar, S., Briand, P., Lupu, R., & Bissell, M. J. Reciprocal interactions between β1-integrin and epidermal growth factor receptor in three-dimensional basement membrane breast cultures: A different perspective in epithelial biology. *Proceedings of the National Academy of Sciences*. (1998)
47. Liu, H., Radisky, D. C., Wang, F., & Bissell, M. J. Polarity and proliferation are controlled by distinct signaling pathways downstream of PI3-kinase in breast epithelial tumor cells. *The Journal of Cell Biology*. (2004)
48. Ciardiello, F. & Tortora, G. EGFR antagonists in cancer treatment. *New England Journal of Medicine*. (2008)
49. Jin, H. & Varner, J. Integrins: roles in cancer development and as treatment targets. *British Journal of Cancer*. (2004)
50. Charette, S. L., McEvoy, L., Pyka, G., Snow-Harter, C., Guido, D., Wiswell, R., &

Marcus, R. Muscle hypertrophy response to resistance training in older women. *Journal of Applied Physiology*. (1991)
51. McCall, G., Byrnes, W., Dickinson, A., Pattany, P., & Fleck, S. Muscle fiber hypertrophy, hyperplasia, and capillary density in college men after resistance training. *Journal of Applied Physiology*. (1996)
52. Wolff, J. Das gesetz der transformation der knochen. *Berlin: Quarto*. (1892)
53. Engler, A. J., Sen, S., Sweeney, H. L., & Discher, D. E. Matrix elasticity directs stem cell lineage specification. *Cell*. (2006)
54. Korn, E. D. Biochemistry of actomyosin-dependent cell motility (a review). *Proceedings of the National Academy of Sciences*. (1978)
55. Discher, D. E., Janmey, P., & Wang, Y. Tissue cells feel and respond to the stiffness of their substrate. *Science*. (2005)
56. Shibue, T. & Weinberg, R. A. Integrin β1-focal adhesion kinase signaling directs the proliferation of metastatic cancer cells disseminated in the lungs. *Proceedings of the National Academy of Sciences*. (2009)
57. Paszek, M. J., Zahir, N., Johnson, K. R., Lakins, J. N., Rozenberg, G. I., Gefen, A., Reinhart-King, C. A., Margulies, S. S., Dembo, M., Boettiger, D., Hammer, D. A., & Weaver, V. M. Tensional homeostasis and the malignant phenotype.. *Cancer Cell*. (2005)
58. Slack-Davis, J. K., Martin, K. H., Tilghman, R. W., Iwanicki, M., Ung, E. J., Autry, C., Luzzio, M. J., Cooper, B., Kath, J. C., & Roberts, W. G. Cellular characterization of a novel focal adhesion kinase inhibitor. *Journal of Biological Chemistry*. (2007)
59. Teixeira, A. I., Abrams, G. A., Bertics, P. J., Murphy, C. J., & Nealey, P. F. Epithelial contact guidance on well-defined micro-and nanostructured substrates. *Journal of Cell Science*. (2003)
60. Patel, A. A., Thakar, R. G., Chown, M., Ayala, P., Desai, T. A., & Kumar, S. Biophysical mechanisms of single-cell interactions with microtopographical cues. *Biomedical Microdevices*. (2010)
61. Lo, C.-M., Wang, H.-B., Dembo, M., & Wang, Y.-l. Cell Movement Is Guided by the Rigidity of the Substrate. *Biophysical Journal*. (2000)
62. Sturgis, J. E., Robinson, J. P., & Voytik-Harbin, S. L. Tensile mechanical properties of three-dimensional type I collagen extracellular matrices with varied microstructure. *Journal of Biomechanical Engineering*. (2002)
63. Vader, D., Kabla, A., Weitz, D., & Mahadevan, L. Strain-Induced Alignment in Collagen Gels. *PLoS ONE*. (2009)
64. Conklin, M. W., Eickhoff, J. C., Riching, K. M., Pehlke, C. A., Eliceiri, K. W., Provenzano, P. P., Friedl, A., & Keely, P. J. Aligned Collagen Is a Prognostic Signature for Survival in Human Breast Carcinoma. *The American Journal of Pathology*. (2011)
65. Provenzano, P. P., Inman, D. R., Eliceiri, K. W., Knittel, J. G., Yan, L., Rueden, C. T., White, J. G., & Keely, P. J. Collagen density promotes mammary tumor initiation and progression. *BMC medicine*. (2008)
66. Provenzano, P., Eliceiri, K., Campbell, J., Inman, D., White, J., & Keely, P. Collagen reorganization at the tumor-stromal interface facilitates local invasion. *BMC Medicine*. (2006)
67. Provenzano, P. P., Inman, D. R., Eliceiri, K. W., Trier, S. M., & Keely, P. J. Contact guidance mediated three-dimensional cell migration is regulated by Rho/ROCK-dependent matrix reorganization. *Biophysical Journal*. (2008)
68. Maruthamuthu, V., Sabass, B., Schwarz, U. S., & Gardel, M. L. Cell-ECM traction force

modulates endogenous tension at cell--cell contacts. *Proceedings of the National Academy of Sciences*. (2011)
69. Dewey Jr, C., Bussolari, S., Gimbrone Jr, M., & Davies, P. The dynamic response of vascular endothelial cells to fluid shear stress.. *Journal of biomechanical engineering*. (1981)
70. Rosenbluth, M. J., Crow, A., Shaevitz, J. W., & Fletcher, D. A. Slow stress propagation in adherent cells. *Biophysical Journal*. (2008)
71. Tse, J. M., Cheng, G., Tyrrell, J. A., Wilcox-Adelman, S. A., Boucher, Y., Jain, R. K., & Munn, L. L. Mechanical compression drives cancer cells toward invasive phenotype. *Proceedings of the National Academy of Sciences*. (2012)
72. Helmlinger, G., Netti, P. A., Lichtenbeld, H. C., Melder, R. J., & Jain, R. K. Solid stress inhibits the growth of multicellular tumor spheroids. *Nat Biotech*. (1997)
73. Cheng, G., Tse, J., Jain, R. K., & Munn, L. L. Micro-Environmental Mechanical Stress Controls Tumor Spheroid Size and Morphology by Suppressing Proliferation and Inducing Apoptosis in Cancer Cells. *PLoS ONE*. (2009)
74. Basan, M., Risler, T., Joanny, J. F., Sastre□Garau, X., & Prost, J. Homeostatic competition drives tumor growth and metastasis nucleation. *HFSP Journal*. (2009)
75. Tanner, K., Mori, H., Mroue, R., Bruni-Cardoso, A., & Bissell, M. J. Coherent angular motion in the establishment of multicellular architecture of glandular tissues. *Proceedings of the National Academy of Sciences*. (2012)
76. Bissell, M., Kenny, P., & Radisky, D. Microenvironmental regulators of tissue structure and function also regulate tumor induction and progression: the role of extracellular matrix and its degrading enzymes. *Cold Spring Harbor Symposia on Quantitative Biology*. (2005)
77. Briand, P., Nielsen, K. V., Madsen, M. W., & Petersen, O. W. Trisomy 7p and malignant transformation of human breast epithelial cells following epidermal growth factor withdrawal. *Cancer Research*. (1996)
78. Cos, S., Fernández, R., Güézmes, A., & Sánchez-Barceló, E. J. Influence of melatonin on invasive and metastatic properties of MCF-7 human breast cancer cells. *Cancer Research*. (1998)
79. Pille, J. Y., Denoyelle, C., Varet, J., Bertrand, J. R., Soria, J., Opolon, P., Lu, H., Pritchard, L. L., Vannier, J. P., & Malvy, C. Anti-RhoA and anti-RhoC siRNAs inhibit the proliferation and invasiveness of MDA-MB-231 breast cancer cells in vitro and in vivo. *Molecular Therapy*. (2005)
80. Miller, F. R., Soule, H. D., Tait, L., Pauley, R. J., Wolman, S. R., Dawson, P. J., & Heppner, G. H. Xenograft model of progressive human proliferative breast disease. *Journal of the National Cancer Institute*. (1993)
81. Basolo, F., Elliott, J., Tait, L., Chen, X. Q., Maloney, T., Russo, I. H., Pauley, R., Momiki, S., Caamano, J., & Klein□Szanto, A. J. P. Transformation of Human Breast Epithelial Cells by c□Ha□ras Oncogene. *Molecular Carcinogenesis*. (2006)
82. Dawson, P. J., Wolman, S. R., Tait, L., Heppner, G. H., & Miller, F. R. MCF10AT: a model for the evolution of cancer from proliferative breast disease.. *The American Journal of Pathology*. (1996)
83. Santner, S. J., Dawson, P. J., Tait, L., Soule, H. D., Eliason, J., Mohamed, A. N., Wolman, S. R., Heppner, G. H., & Miller, F. R. Malignant MCF10CA1 cell lines derived from premalignant human breast epithelial MCF10AT cells. *Breast Cancer Research and Treatment*. (2001)
84. Butcher, D. T., Alliston, T., & Weaver, V. M. A tense situation: forcing tumour

progression. *Nature Reviews Cancer*. (2009)
85. Wells, R. G. The role of matrix stiffness in regulating cell behavior. *Hepatology*. (2008)
86. Bissell, M. J., Rizki, A., & Mian, I. S. Tissue architecture: the ultimate regulator of breast epithelial function. *Current Opinion in Cell Biology*. (2003)
87. Falconnet, D., Csucs, G., Michelle Grandin, H., & Textor, M. Surface engineering approaches to micropattern surfaces for cell-based assays. *Biomaterials*. (2006)
88. Brown, T. D. Techniques for mechanical stimulation of cells in vitro: a review. *Journal of Biomechanics*. (2000)
89. Fournier, M. V., Fata, J. E., Martin, K. J., Yaswen, P., & Bissell, M. J. Interaction of E-cadherin and PTEN regulates morphogenesis and growth arrest in human mammary epithelial cells. *Cancer Research*. (2009)
90. Chen, C. S., Mrksich, M., Huang, S., Whitesides, G. M., & Ingber, D. E. Geometric control of cell life and death. *Science*. (1997)
91. Lehnert, D., Wehrle-Haller, B., David, C., Weiland, U., Ballestrem, C., Imhof, B. A., & Bastmeyer, M. Cell behaviour on micropatterned substrata: limits of extracellular matrix geometry for spreading and adhesion. *Journal of Cell Science*. (2004)
92. Singhvi, R., Kumar, A., Lopez, G. P., Stephanopoulos, G. N., Wang, D., Whitesides, G. M., & Ingber, D. E. Engineering cell shape and function.. *Science*. (1994)
93. Tan, J. L., Liu, W., Nelson, C. M., Raghavan, S., & Chen, C. S. Simple approach to micropattern cells on common culture substrates by tuning substrate wettability. *Tissue Engineering*. (2004)
94. Nelson, C. M., Khauv, D., Bissell, M. J., & Radisky, D. C. Change in cell shape is required for matrix metalloproteinase□induced epithelial□mesenchymal transition of mammary epithelial cells. *Journal of cellular biochemistry*. (2008)
95. Bhowmick, N. A., Ghiassi, M., Bakin, A., Aakre, M., Lundquist, C. A., Engel, M. E., Arteaga, C. L., & Moses, H. L. Transforming growth factor-β1 mediates epithelial to mesenchymal transdifferentiation through a RhoA-dependent mechanism. *Molecular Biology of the Cell*. (2001)
96. Kaufman, L., Brangwynne, C., Kasza, K., Filippidi, E., Gordon, V., Deisboeck, T., & Weitz, D. Glioma expansion in collagen I matrices: analyzing collagen concentration-dependent growth and motility patterns. *Biophysical Journal*. (2005)
97. Raub, C. B., Suresh, V., Krasieva, T., Lyubovitsky, J., Mih, J. D., Putnam, A. J., Tromberg, B. J., & George, S. C. Noninvasive assessment of collagen gel microstructure and mechanics using multiphoton microscopy. *Biophysical Journal*. (2007)
98. Ulrich, T. A., Jain, A., Tanner, K., MacKay, J. L., & Kumar, S. Probing cellular mechanobiology in three-dimensional culture with collagen--agarose matrices. *Biomaterials*. (2010)
99. Fischbach, C., Kong, H. J., Hsiong, S. X., Evangelista, M. B., Yuen, W., & Mooney, D. J. Cancer cell angiogenic capability is regulated by 3D culture and integrin engagement. *Science Signaling*. (2009)
100. Crow, A., Webster, K., Hohlfeld, E., Ng, W., Geissler, P., & Fletcher, D. Contractile Equilibration of Single Cells to Step Changes in Extracellular Stiffness. *Biophysical Journal*. (2012)
101. Yeung, T., Georges, P. C., Flanagan, L. A., Marg, B., Ortiz, M., Funaki, M., Zahir, N., Ming, W., Weaver, V., & Janmey, P. A. Effects of substrate stiffness on cell morphology, cytoskeletal structure, and adhesion. *Cell Motility and the Cytoskeleton*. (2004)

102. Engler, A., Bacakova, L., Newman, C., Hategan, A., Griffin, M., & Discher, D. Substrate compliance versus ligand density in cell on gel responses. *Biophysical Journal*. (2004)
103. Dupont, S., Morsut, L., Aragona, M., Enzo, E., Giulitti, S., Cordenonsi, M., Zanconato, F., Le Digabel, J., Forcato, M., & Bicciato, S. Role of YAP/TAZ in mechanotransduction. *Nature*. (2011)
104. Bonassar, L. J., Grodzinsky, A. J., Frank, E. H., Davila, S. G., Bhaktav, N. R., & Trippel, S. B. The effect of dynamic compression on the response of articular cartilage to insulin-like growth factor-I. *Journal of Orthopaedic Research*. (2006)
105. Bonnel, F., Peruchon, E., Baldet, P., Dimeglio, A., & Rabischong, P. Effects of compression on growth plates in the rabbit. *Acta Orthopaedica*. (1983)
106. Gupta, R. & Steward, O. Chronic nerve compression induces concurrent apoptosis and proliferation of Schwann cells. *The Journal of Comparative Neurology*. (2003)
107. Lulevich, V., Zink, T., Chen, H. Y., Liu, F. T., & Liu, G. Cell mechanics using atomic force microscopy-based single-cell compression. *Langmuir*. (2006)
108. Dao, M., Lim, C. T., & Suresh, S. Mechanics of the human red blood cell deformed by optical tweezers. *Journal of the Mechanics and Physics of Solids*. (2003)
109. le Duc, Q., Shi, Q., Blonk, I., Sonnenberg, A., Wang, N., Leckband, D., & de Rooij, J. Vinculin potentiates E-cadherin mechanosensing and is recruited to actin-anchored sites within adherens junctions in a myosin II--dependent manner. *The Journal of Cell Biology*. (2010)
110. Chaudhuri, O., Parekh, S. H., Lam, W. A., & Fletcher, D. A. Combined atomic force microscopy and side-view optical imaging for mechanical studies of cells. *Nature Methods*. (2009)
111. Chaudhuri, O., Parekh, S. H., & Fletcher, D. A. Reversible stress softening of actin networks. *Nature*. (2007)
112. Parekh, S. H., Chaudhuri, O., Theriot, J. A., & Fletcher, D. A. Loading history determines the velocity of actin-network growth. *Nature Cell Biology*. (2005)
113. Vlahakis, N. E., Schroeder, M. A., Limper, A. H., & Hubmayr, R. D. Stretch induces cytokine release by alveolar epithelial cells in vitro. *American Journal of Physiology-Lung Cellular and Molecular Physiology*. (1999)
114. Provenzano, P. P., Inman, D. R., Eliceiri, K. W., & Keely, P. J. Matrix density-induced mechanoregulation of breast cell phenotype, signaling and gene expression through a FAK-ERK linkage. *Oncogene*. (2009)
115. Evans, E. A. Bending elastic modulus of red blood cell membrane derived from buckling instability in micropipet aspiration tests. *Biophysical Journal*. (1983)
116. Guevorkian, K., Gonzalez-Rodriguez, D., Carlier, C., Dufour, S., & Brochard-Wyart, F. Mechanosensitive shivering of model tissues under controlled aspiration. *Proceedings of the National Academy of Sciences*. (2011)
117. Girton, T. S., Barocas, V. H., & Tranquillo, R. T. Confined Compression of a Tissue-Equivalent: Collagen Fibril and Cell Alignment in Response to Anisotropic Strain. *Journal of Biomechanical Engineering*. (2002)
118. Shaikh, F. M., O'Brien, T. P., Callanan, A., Kavanagh, E. G., Burke, P. E., Grace, P. A., & McGloughlin, T. M. New Pulsatile Hydrostatic Pressure Bioreactor for Vascular Tissue-Engineered Constructs. *Artificial Organs*. (2010)
119. Gjorevski, N. & Nelson, C. M. Branch formation during organ development. *Wiley Interdisciplinary Reviews: Systems Biology and Medicine*. (2010)
120. Propper, A. & Gomot, L. Control of chick epidermis differentiation by rabbit mammary

mesenchyme. *Cellular and Molecular Life Sciences*. (1973)
121. Sakakura, T., Nishizuka, Y., & Dawe, C. Mesenchyme-dependent morphogenesis and epithelium-specific cytodifferentiation in mouse mammary gland. *Science*. (1976)
122. Cunha, G. R., Young, P., Christov, K., Guzman, R., Nandi, S., Talamantes, F., & Thordarson, G. Mammary Phenotypic Expression Induced in Epidermal Cells by Embryonic Mammary Mesenchyme. *Cells Tissues Organs*. (1995)
123. Ingman, W. V., Wyckoff, J., Gouon-Evans, V., Condeelis, J., & Pollard, J. W. Macrophages promote collagen fibrillogenesis around terminal end buds of the developing mammary gland. *Developmental Dynamics*. (2006)
124. Ridley, A. J., Paterson, H. F., Johnston, C. L., Diekmann, D., & Hall, A. The small GTP-binding protein rac regulates growth factor-induced membrane ruffling. *Cell*. (1992)
125. Machesky, L. M. & Hall, A. Role of Actin Polymerization and Adhesion to Extracellular Matrix in Rac- and Rho-induced Cytoskeletal Reorganization. *The Journal of Cell Biology*. (1997)
126. Kureishy, N., Sapountzi, V., Prag, S., Anilkumar, N., & Adams, J. C. Fascins, and their roles in cell structure and function. *BioEssays*. (2002)
127. Wozniak, M. A., Desai, R., Solski, P. A., Der, C. J., & Keely, P. J. ROCK-generated contractility regulates breast epithelial cell differentiation in response to the physical properties of a three-dimensional collagen matrix. *The Journal of Cell Biology*. (2003)
128. Bissell, M. J., Hall, H. G., & Parry, G. How does the extracellular matrix direct gene expression?. *Journal of Theoretical Biology*. (1982)
129. Nelson, C. M. & Bissell, M. J. Of Extracellular Matrix, Scaffolds, and Signaling: Tissue Architecture Regulates Development, Homeostasis, and Cancer. *Annual Review of Cell and Developmental Biology*. (2006)
130. Keely, P. J., Wu, J. E., & Santoro, S. A. The spatial and temporal expression of the α2β1 integrin and its ligands, collagen I, collagen IV, and laminin, suggest important roles in mouse mammary morphogenesis. *Differentiation*. (1995)
131. Talhouk, R. S., Chin, J. R., Unemori, E. N., Werb, Z., & Bissell, M. J. Proteinases of the mammary gland: developmental regulation in vivo and vectorial secretion in culture. *Development*. (1991)
132. Schedin, P., Mitrenga, T., McDaniel, S., & Kaeck, M. Mammary ECM composition and function are altered by reproductive state. *Molecular Carcinogenesis*. (2004)
133. Wicha, M. S., Liotta, L. A., Vonderhaar, B. K., & Kidwell, W. R. Effects of inhibition of basement membrane collagen deposition on rat mammary gland development. *Developmental Biology*. (1980)
134. Stopak, D., Wessells, N. K., & Harris, A. K. Morphogenetic rearrangement of injected collagen in developing chicken limb buds. *Proceedings of the National Academy of Sciences*. (1985)
135. Guo, C. & Kaufman, L. J. Flow and magnetic field induced collagen alignment. *Biomaterials*. (2007)
136. Tower, T. T., Neidert, M. R., & Tranquillo, R. T. Fiber Alignment Imaging During Mechanical Testing of Soft Tissues. *Annals of Biomedical Engineering*. (2002-11-01)
137. Pankov, R., Endo, Y., Even-Ram, S., Araki, M., Clark, K., Cukierman, E., Matsumoto, K., & Yamada, K. M. A Rac switch regulates random versus directionally persistent cell migration. *Journal of Cell Biology*. (2005)
138. Xia, N., Thodeti, C. K., Hunt, T. P., Xu, Q., Ho, M., Whitesides, G. M., Westervelt, R., &

Ingber, D. E. Directional control of cell motility through focal adhesion positioning and spatial control of Rac activation. *The FASEB Journal*. (2008)
139. Migeotte, I., Omelchenko, T., Hall, A., & Anderson, K. V. Rac1-Dependent Collective Cell Migration Is Required for Specification of the Anterior-Posterior Body Axis of the Mouse. *PLoS Biology*. (2010)
140. Adams, J. C. & Schwartz, M. A. Stimulation of Fascin Spikes by Thrombospondin-1 Is Mediated by the Gtpases Rac and Cdc42. *The Journal of Cell Biology*. (2000)
141. Parsons, M. & Adams, J. C. Rac regulates the interaction of fascin with protein kinase C in cell migration. *Journal of Cell Science*. (2008)
142. Hashimoto, Y., Parsons, M., & Adams, J. C. Dual Actin-bundling and Protein Kinase C-binding Activities of Fascin Regulate Carcinoma Cell Migration Downstream of Rac and Contribute to Metastasis. *Molecular Biology of the Cell*. (2007)
143. Guo, C.-L., Ouyang, M., Yu, J.-Y., Maslov, J., Price, A., & Shen, C.-Y. Long-range mechanical force enables self-assembly of epithelial tubular patterns. *Proceedings of the National Academy of Sciences*. (2012)
144. Vargo-Gogola, T., Heckman, B. M., Gunther, E. J., Chodosh, L. A., & Rosen, J. M. P190-B Rho GTPase-Activating Protein Overexpression Disrupts Ductal Morphogenesis and Induces Hyperplastic Lesions in the Developing Mammary Gland. *Molecular Endocrinology*. (2006)
145. Krahn, K. N., Bouten, C. V. C., van Tuijl, S., van Zandvoort, M. A. M. J., & Merkx, M. Fluorescently labeled collagen binding proteins allow specific visualization of collagen in tissues and live cell culture. *Analytical Biochemistry*. (2006)
146. Boerboom, R. A., Krahn, K. N., Megens, R. T. A., van Zandvoort, M. A. M. J., Merkx, M., & Bouten, C. V. C. High resolution imaging of collagen organisation and synthesis using a versatile collagen specific probe. *Journal of Structural Biology*. (2007)
147. Fata, J. E., Mori, H., Ewald, A. J., Zhang, H., Yao, E., Werb, Z., & Bissell, M. J. The MAPKERK-1,2 pathway integrates distinct and antagonistic signals from TGFαand FGF7 in morphogenesis of mouse mammary epithelium. *Developmental Biology*. (2007)
148. Pujuguet, P., Radisky, D., Levy, D., Lacza, C., & Bissell, M. J. Trichostatin a inhibits β-casein expression in mammary epithelial cells. *Journal of Cellular Biochemistry*. (2001)
149. Rezakhaniha, R., Agianniotis, A., Schrauwen, J., Griffa, A., Sage, D., Bouten, C., van de Vosse, F., Unser, M., & Stergiopulos, N. Experimental investigation of collagen waviness and orientation in the arterial adventitia using confocal laser scanning microscopy. *Biomechanics and Modeling in Mechanobiology*. (2012)
150. Briand, P., Petersen, O. W., & Van Deurs, B. A new diploid nontumorigenic human breast epithelial cell line isolated and propagated in chemically defined medium. *In Vitro Cell Dev Biol*. (1987)
151. Petersen, O. W., Rønnov-Jessen, L., Howlett, A. R., & Bissell, M. J. Interaction with basement membrane serves to rapidly distinguish growth and differentiation pattern of normal and malignant human breast epithelial cells. *Proceedings of the National Academy of Sciences*. (1992)
152. Rizki, A., Weaver, V. M., Lee, S.-Y., Rozenberg, G. I., Chin, K., Myers, C. A., Bascom, J. L., Mott, J. D., Semeiks, J. R., Grate, L. R., Mian, I. S., Borowsky, A. D., Jensen, R. A., Idowu, M. O., Chen, F., Chen, D. J., Petersen, O. W., Gray, J. W., & Bissell, M. J. A human breast cell model of preinvasive to invasive transition. *Cancer Research*. (2008)
153. Murata, M., Bonassar, L. J., Wright, M., Mankin, H. J., & Towle, C. A. A role for the

interleukin-1 receptor in the pathway linking static mechanical compression to decreased proteoglycan synthesis in surface articular cartilage. *Archives of Biochemistry and Biophysics*. (2003)
154. Chamay, A. & Tschantz, P. Mechanical influences in bone remodeling. Experimental research on Wolff's law. *Journal of Biomechanics*. (1972)
155. Cheng, J. C. Y., Evans, J. H., Leung, K. S., Clark, J. A., Choy, T. T. C., & Leung, P. C. Pressure therapy in the treatment of post-burn hypertrophic scar - A critical look into its usefulness and fallacies by pressure monitoring. *Burns*. (1984)
156. In vitro mechanical compression induces apoptosis and regulates cytokines release in hypertrophic scars. *Wound Repair and Regeneration*. (2003)
157. Pryse, K. M., Nekouzadeh, A., Genin, G. M., Elson, E. L., & Zahalak, G. I. Incremental mechanics of collagen gels: new experiments and a new viscoelastic model. *Annals of Biomedical Engineering*. (2003)
158. Allen, P., Melero-Martin, J., & Bischoff, J. Type I collagen, fibrin and PuraMatrix matrices provide permissive environments for human endothelial and mesenchymal progenitor cells to form neovascular networks. *Journal of Tissue Engineering and Regenerative Medicine*. (2011)
159. Watabe, M., Nagafuchi, A., Tsukita, S., & Takeichi, M. Induction of polarized cell-cell association and retardation of growth by activation of the E-cadherin-catenin adhesion system in a dispersed carcinoma line. *J Cell Biol*. (1994)
160. Wang, F., Hansen, R. K., Radisky, D., Yoneda, T., Barcellos-Hoff, M. H., Petersen, O. W., Turley, E. A., & Bissell, M. J. Phenotypic Reversion or Death of Cancer Cells by Altering Signaling Pathways in Three-Dimensional Contexts. *Journal of the National Cancer Institute*. (2002)
161. Talhouk, R. S., Bissell, M. J., & Werb, Z. Coordinated expression of extracellular matrix-degrading proteinases and their inhibitors regulates mammary epithelial function during involution. *Journal of Cell Biology*. (1992)
162. Munevar, S., Wang, Y., & Dembo, M. Traction force microscopy of migrating normal and H-ras transformed 3T3 fibroblasts. *Biophysical Journal*. (2001)
163. Kim, J. H. & Asthagiri, A. R. Matrix stiffening sensitizes epithelial cells to EGF and enables the loss of contact inhibition of proliferation. *Journal of Cell Science*. (2011)
164. Boussadia, O., Kutsch, S., Hierholzer, A., Delmas, V., & Kemler, R. E-cadherin is a survival factor for the lactating mouse mammary gland. *Mechanisms of Development*. (2002)
165. Virnig, B. A., Tuttle, T. M., Shamliyan, T., & Kane, R. L. Ductal Carcinoma In Situ of the Breast: A Systematic Review of Incidence, Treatment, and Outcomes. *Journal of the National Cancer Institute*. (2010)
166. Li, Q., Lee, G., Ong, C., & Lim, C. AFM indentation study of breast cancer cells. *Biochemical and Biophysical Research Communications*. (2008)
167. von Dassow, M., Strother, J. A., & Davidson, L. A. Surprisingly simple mechanical behavior of a complex embryonic tissue. *PLoS One*. (2010)
168. Soule, H. D., Maloney, T. M., Wolman, S. R., Peterson, W. D., Brenz, R., McGrath, C. M., Russo, J., Pauley, R. J., Jones, R. F., & Brooks, S. Isolation and characterization of a spontaneously immortalized human breast epithelial cell line, MCF-10. *Cancer Research*. (1990)
169. Barocas, V. H., Moon, A. G., & Tranquillo, R. T. The fibroblast-populated collagen microsphere assay of cell traction force--Part 2: Measurement of the cell traction parameter..

Journal of Biomechanical Engineering. (1995)
170. Dembo, M. & Harlow, F. Cell motion, contractile networks, and the physics of interpenetrating reactive flow. *Biophysical Journal*. (1986)
171. Herant, M., Marganski, W. A., & Dembo, M. The mechanics of neutrophils: synthetic modeling of three experiments. *Biophysical Journal*. (2003)
172. Herant, M. & Dembo, M. Form and function in cell motility: from fibroblasts to keratocytes. *Biophysical Journal*. (2010)
173. Moon, A. G. & Tranquillo, R. T. Fibroblast□populated collagen microsphere assay of cell traction force: Part 1. Continuum model. *AIChE journal*. (2004)
174. Sethian, J. A. Level set methods and fast marching methods: evolving interfaces in computational geometry, fluid mechanics, computer vision, and materials science. . (1999)
175. Plopper, G. & Ingber, D. E. Rapid induction and isolation of focal adhesion complexes. *Biochemical and Biophysical Research Communications*. (1993)
176. Chorin, A. J. Numerical solution of the Navier-Stokes equations. *Math. Comp*. (1968)
177. Almgren, A. S., Bell, J. B., & Szymczak, W. G. A numerical method for the incompressible Navier-Stokes equations based on an approximate projection. *SIAM Journal on Scientific Computing*. (1996)
178. Kita-Matsuo, H., Barcova, M., Prigozhina, N., Salomonis, N., Wei, K., Jacot, J. G., Nelson, B., Spiering, S., Haverslag, R., & Kim, C. Lentiviral vectors and protocols for creation of stable hESC lines for fluorescent tracking and drug resistance selection of cardiomyocytes. *PLoS One*. (2009)
179. Chrzanowska-Wodnicka, M. & Burridge, K. Rho-stimulated contractility drives the formation of stress fibers and focal adhesions.. *Journal of Cell Biology*. (1996)
180. Vignjevic, D., Kojima, S., Aratyn, Y., Danciu, O., Svitkina, T., & Borisy, G. G. Role of fascin in filopodial protrusion. *Journal of Cell Biology*. (2006)
181. Mortazavi, A., Williams, B. A., McCue, K., Schaeffer, L., & Wold, B. Mapping and quantifying mammalian transcriptomes by RNA-Seq. *Nature Methods*. (2008)
182. Wang, Z., Gerstein, M., & Snyder, M. RNA-Seq: a revolutionary tool for transcriptomics. *Nature Reviews Genetics*. (2009)
183. Novak, R., Zeng, Y., Shuga, J., Venugopalan, G., Fletcher, D. A., Smith, M. T., & Mathies, R. A. Single-Cell Multiplex Gene Detection and Sequencing with Microfluidically Generated Agarose Emulsions. *Angewandte Chemie*. (2011)
184. Santangelo, P. J., Nix, B., Tsourkas, A., & Bao, G. Dual FRET molecular beacons for mRNA detection in living cells. *Nucleic Acids Research*. (2004)
185. Bulun, S., Price, T., Aitken, J., Mahendroo, M., & Simpson, E. A link between breast cancer and local estrogen biosynthesis suggested by quantification of breast adipose tissue aromatase cytochrome P450 transcripts using competitive polymerase chain reaction after reverse transcription.. *Journal of Clinical Endocrinology & Metabolism*. (1993)
186. Päth, G., Bornstein, S. R., Gurniak, M., Chrousos, G. P., Scherbaum, W. A., & Hauner, H. Human breast adipocytes express interleukin-6 (IL-6) and its receptor system: increased IL-6 production by β-adrenergic activation and effects of IL-6 on adipocyte function. *Journal of Clinical Endocrinology & Metabolism*. (2001)
187. Huss, F. R. M. & Kratz, G. Mammary epithelial cell and adipocyte co-culture in a 3-D matrix: the first step towards tissue-engineered human breast tissue. *Cells Tissues Organs*. (2001)
188. Manabe, Y., Toda, S., Miyazaki, K., & Sugihara, H. Mature adipocytes, but not

preadipocytes, promote the growth of breast carcinoma cells in collagen gel matrix culture through cancer-stromal cell interactions. *The Journal of Pathology*. (2003)
189. Larsson, T., Aspden, R., & Heinegård, D. Effects of mechanical load on cartilage matrix biosynthesis in vitro. *Matrix*. (1991)
190. Furuta, S., Jeng, Y. M., Zhou, L., Huang, L., Kuhn, I., Bissell, M. J., & Lee, W. H. IL-25 Causes Apoptosis of IL-25R--Expressing Breast Cancer Cells Without Toxicity to Nonmalignant Cells. *Science Translational Medicine*. (2011)